



# Face Gear Drive With Helical Involute Pinion: Geometry, Generation by a Shaper and a Worm, Avoidance of Singularities and Stress Analysis

Faydor L. Litvin  
University of Chicago, Chicago, Illinois

Alfonso Fuentes  
Polytechnic University of Cartagena, Spain

Ignacio Gonzalez-Perez, Alessandro Piscopo, and Paolo Ruzziconi  
University of Chicago, Chicago, Illinois

## The NASA STI Program Office . . . in Profile

Since its founding, NASA has been dedicated to the advancement of aeronautics and space science. The NASA Scientific and Technical Information (STI) Program Office plays a key part in helping NASA maintain this important role.

The NASA STI Program Office is operated by Langley Research Center, the Lead Center for NASA's scientific and technical information. The NASA STI Program Office provides access to the NASA STI Database, the largest collection of aeronautical and space science STI in the world. The Program Office is also NASA's institutional mechanism for disseminating the results of its research and development activities. These results are published by NASA in the NASA STI Report Series, which includes the following report types:

- **TECHNICAL PUBLICATION.** Reports of completed research or a major significant phase of research that present the results of NASA programs and include extensive data or theoretical analysis. Includes compilations of significant scientific and technical data and information deemed to be of continuing reference value. NASA's counterpart of peer-reviewed formal professional papers but has less stringent limitations on manuscript length and extent of graphic presentations.
- **TECHNICAL MEMORANDUM.** Scientific and technical findings that are preliminary or of specialized interest, e.g., quick release reports, working papers, and bibliographies that contain minimal annotation. Does not contain extensive analysis.
- **CONTRACTOR REPORT.** Scientific and technical findings by NASA-sponsored contractors and grantees.

- **CONFERENCE PUBLICATION.** Collected papers from scientific and technical conferences, symposia, seminars, or other meetings sponsored or cosponsored by NASA.
- **SPECIAL PUBLICATION.** Scientific, technical, or historical information from NASA programs, projects, and missions, often concerned with subjects having substantial public interest.
- **TECHNICAL TRANSLATION.** English-language translations of foreign scientific and technical material pertinent to NASA's mission.

Specialized services that complement the STI Program Office's diverse offerings include creating custom thesauri, building customized databases, organizing and publishing research results . . . even providing videos.

For more information about the NASA STI Program Office, see the following:

- Access the NASA STI Program Home Page at <http://www.sti.nasa.gov>
- E-mail your question via the Internet to [help@sti.nasa.gov](mailto:help@sti.nasa.gov)
- Fax your question to the NASA Access Help Desk at 301-621-0134
- Telephone the NASA Access Help Desk at 301-621-0390
- Write to:  
NASA Access Help Desk  
NASA Center for AeroSpace Information  
7121 Standard Drive  
Hanover, MD 21076



# Face Gear Drive With Helical Involute Pinion: Geometry, Generation by a Shaper and a Worm, Avoidance of Singularities and Stress Analysis

Faydor L. Litvin  
University of Chicago, Chicago, Illinois

Alfonso Fuentes  
Polytechnic University of Cartagena, Spain

Ignacio Gonzalez-Perez, Alessandro Piscopo, and Paolo Ruzziconi  
University of Chicago, Chicago, Illinois

Prepared under Grant NAG3-2450

National Aeronautics and  
Space Administration

Glenn Research Center

## Acknowledgments

The authors express their deep gratitude to NASA Glenn Research Center, Army Research Laboratory and Gleason Foundation for the financial support of this project.

Available from

NASA Center for Aerospace Information  
7121 Standard Drive  
Hanover, MD 21076

National Technical Information Service  
5285 Port Royal Road  
Springfield, VA 22100

Available electronically at <http://gltrs.grc.nasa.gov>

# Face Gear Drive with Helical Involute Pinion: Geometry, Generation by a Shaper and a Worm, Avoidance of Singularities and Stress Analysis

Faydor L. Litvin  
University of Chicago  
Chicago, Illinois 60607

Alfonso Fuentes  
Polytechnic University of Cartagena  
Spain

Ignacio Gonzalez-Perez, Alessandro Piscopo, and Paolo Ruzziconi  
University of Chicago  
Chicago, Illinois 60607

A new type of face-gear drive with intersected axes of rotation formed by a helical involute pinion and conjugated face-gear has been investigated. Generation of face-gears by a shaper free of undercutting and pointing has been investigated. A new method of grinding or cutting of face-gears by a worm of special shape has been developed. A computerized design procedure has been developed to avoid undercutting and pointing by a shaper or by a generating worm. Also, a method to determine the limitations of the helix angle magnitude has been developed. The method provides a localization of the bearing contact to reduce the shift of bearing contact caused by misalignment. The analytical method provides a simulation of the meshing and contact of misaligned gear drives. An automatic mesh generation method has been developed and used to conduct a 3-D contact stress analysis of several teeth. The theory developed is illustrated with several examples.

## Nomenclature

$\alpha_n$	Normal pressure angle (fig. 5(b))
$\alpha_c$	Cross pressure angle (fig. 3)
$\beta$	Skew angle of rack-cutter (figs. 5(a)), helix angle (fig. 13)
$s_0, v_0$	Space and width of the teeth of the rack-cutter (fig. 5(b))
$\lambda_c$	Rack-cutter parameter
$(u_i, l_i)$ (i = 1, s)	Surface parameters (figs. 5(a) and (b))
$(\theta_i, \varepsilon_i)$ (i = 1, s)	Surface parameters (figs. 3 and 4)
$\gamma_m$	Shaft angle between the shaper and the face-gear (figs. 7, 24, and 25)
$\Delta\gamma_m$	Shaft angle error (figs. 24(c) and 25)
$\Delta E$	Shortest distance error between the pinion and the face-gear axes (fig. 24(b))
$\Delta q$	Axial displacement of face gear (figs. 24(c) and 25)
$\lambda_w$	Lead angle of the worm (fig. 13)
$\gamma_{ws}$	Crossing angle between axes of shaper and worm (figs. 12, 13, and 22)
$\eta_s$	Half of the width of the space on the base cylinder (fig. 3)

$\Sigma_i$ ( $i = s, 1, 2, w$ )	Tooth surface of the shaper ( $i = s$ ), pinion ( $i = 1$ ), face-gear ( $i = 2$ ), and generating worm ( $i = w$ )
$\Psi_i$ ( $i = s, 2, w$ )	Angles of rotation of the shaper ( $i = s$ ), face gear ( $i = 2$ ), and worm ( $i = w$ ) formed during the process of generation
$\phi_i$ ( $i = 1, 2$ )	Angles of rotation of the pinion ( $i = 1$ ) and the face gear ( $i = 2$ ) formed during the process of meshing (figs. 24(a) and (d))
$E_{ws}$	Shortest distance between the axes of the shaper and the worm (figs. 11, 12, and 22)
$L_i$ ( $i = 1, 2$ )	Inner ( $i = 1$ ) and outer ( $i = 2$ ) limiting dimensions of the face gear (fig. 7(a))
$M_{ji}, L_{ji}$	Matrices $4 \times 4$ and $3 \times 3$ for transformation from $S_i$ to $S_j$ of point coordinates and vectors
$m$	Module
$N_i$ ( $i = s, 1, 2, w$ )	Number of teeth of the shaper ( $i = s$ ), pinion ( $i = 1$ ), face-gear ( $i = 2$ ), and generating worm ( $i = w$ )
$P_d$	Diametral pitch
$r_{pi}$ ( $i = 1, s$ )	Radius of the pitch circle of the pinion (shaper) (figs. 3, and 5(c))
$r_{bi}$ ( $i = 1, s$ )	Radius of the base cylinder of the pinion (shaper) (fig. 3)
$r_{pw}$	Radius of the pitch circle of the worm (fig. 11)

## 1. Introduction

Face gear drives have found application in helicopter transmissions. Figure 1 shows an example of a design wherein the driving pinion is simultaneously in mesh with two face-gears. Such a design permits splitting of the torque between two face-gears. This leads to a transmission design with reduced weight. Design of face-gear drives with a spur pinion was the subject of the research of many designers, for instance, [13, 17, 18]. However, the previous design was limited by application of a spur pinion. The new approach developed includes application of a face-gear drive with a helical pinion (fig. 2) for the reduction of contact stresses and increase contact ratio.

There are many opportunities to apply face-gear drives in transmissions. Face-gear drives in comparison with hypoid gears drives and spiral bevel gears can provide a higher gear ratio

$m_{12} = \omega^{(1)} / \omega^{(2)}$ . The transformation of rotation by face-gear drives is performed between intersected axes wherein hypoid gear drives perform rotation between crossed axes. Therefore, the efficiency of face-gear drives is expected to be higher in comparison with hypoid gear drives.

A new approach has been developed for generation and manufacture of a face gear conjugated to an involute helical pinion, in addition to generation by a shaper. The new approach is based on application of a grinding worm or cutting worm of a special shape. In the previous design, generation of face-gear by a worm has been limited to the case of application of a spur involute pinion as the driving member of the drive. Application of a screw involute pinion has required a new approach that is based on two-parameters enveloping of generation of the face-gear by a worm (see section 5).

The report covers as well avoidance of singularities and undercutting of the face-gear and the grinding worm. A special attention is based on the development of an enhanced approach to stress analysis. This approach provides automatization of the contact model development and investigation of formation of the bearing contact during the cycle of meshing.

The developed theory is illustrated with numerical examples. The performed research is based on application of modern theory of gearing that has been a subject of research by Zalgaller [24], Zalgaller

and Litvin [25], Stosic and co-authors [21, 22, 23], Bar [4], Shevelova [19], Baumann [3], Stadtfeld [20], and Litvin and his followers [1, 2, 7, 8, 9, 10, 11, 12, 14, 15].

## 2. Derivation of Surfaces of Helical Pinion and Helical Shaper

The helical pinion is the driving member of the face-gear drive. Two methods of generation of the face-gear are considered: (i) by application of a helical shaper (see section 3), and (ii) by application of a worm of a special shape (see sections 4 and 5). The shaper and the face-gear are in instantaneous line contact while the pinion and the face-gear are in instantaneous point contact. The bearing contact of the pinion and the face-gear is localized because the number  $N_1$  of the teeth of the pinion is less than the number  $N_s$  of the teeth of the shaper:  $N_s - N_1 = 2$  or  $3$ .

The derivation of the equations of the tooth surface of the pinion and the shaper is based on two alternative approaches:

### Approach 1

1. The transverse-profiles of the pinion (or the shaper) are considered as involute profiles represented in coordinate system  $S_q^{(i)}$  ( $i = 1, s$ ).

2. The tooth surface  $\Sigma_i$  ( $i = 1, s$ ) is generated while coordinate system  $S_q^{(i)}$  ( $i = 1, s$ ) (together with the transverse-profiles) performs a screw motion about the axis  $z_i$  ( $i = 1, s$ ) of the pinion (the shaper).

The transverse-profiles are represented in coordinate system  $S_q^{(i)}$  by the equations (fig. 3).

$$\begin{aligned} x_q^{(i)}(\theta_i) &= r_{bi} \left[ \cos(\theta_i + \eta_i) + \theta_i \sin(\theta_i + \eta_i) \right] \\ y_q^{(i)}(\theta_i) &= r_{bi} \left[ \pm \sin(\theta_i + \eta_i) \mp \theta_i \sin(\theta_i + \eta_i) \right] \\ z_q^{(i)}(\theta_i) &= 0 \end{aligned} \quad (1)$$

Here,  $r_{bi}$  is the radius of the base cylinder;  $\theta_i \frac{1}{2}$  is the parameter of involute profile; the angle  $2\eta_i$  corresponds to the width of the space on the base cylinder between the two profiles. The upper and lower signs correspond to profile I and II, respectively.

The screw involute surface of the shaper is represented in  $S_i$  (fig. 4) by the following matrix equation

$$r_i(\varepsilon_i, \theta_i) = M_{iq}^{(i)}(\varepsilon_i) r_q^{(i)}(\theta_i) \quad (2)$$

where  $\varepsilon_i$  is the angle of rotation in the screw motion of  $S_q^{(i)}$  with respect to  $S_i$  ( $i = 1, s$ ). Then, we obtain the following equations of the tooth surface

$$\begin{aligned} x_i(\varepsilon_i, \theta_i) &= r_{bi} \left[ \cos \left[ (\theta_i + \eta_i) \mp \varepsilon_i \right] + \theta_i \sin \left[ (\theta_i + \eta_i) \mp \varepsilon_i \right] \right] \triangleleft \\ y_i(\varepsilon_i, \theta_i) &= r_{bi} \left[ \pm \sin \left[ (\theta_i + \eta_i) \mp \varepsilon_i \right] \mp \theta_i \cos \left[ (\theta_i + \eta_i) \mp \varepsilon_i \right] \right] \\ z_i(\varepsilon_i) &= p_i \varepsilon_i \end{aligned} \quad (3)$$

where  $p_i$  is the screw parameter. The surface normal is represented as:

$$\mathbf{N}_i(\theta_i, \varepsilon_i) = \frac{\partial \mathbf{r}_i}{\partial \theta_i} \times \frac{\partial \mathbf{r}_i}{\partial \varepsilon_i} \quad (4)$$

## Approach 2

The helical pinion and helical shaper surfaces  $\Sigma_i$  ( $i = 1, s$ ) may be generated as well as the envelope to the family of surfaces  $\Sigma_c$  of a generating skew rack-cutter.

Figure 5(a) shows such a surface where  $\beta$  is the skew angle. Here, the normal section  $a-a$  and the transverse section  $b-b$  are obtained by planes that are perpendicular to plane  $\Pi$  and have the orientation  $a-a$  and  $b-b$ , respectively. Orientation  $a-a$  is determined by angle  $\beta$ . Figure 5(b) shows the normal section  $a-a$ , where  $\alpha_n$  is the normal pressure angle,  $s_0$  and  $w_0$  represent the space and the tooth width, respectively, of the rack-cutter tooth. Magnitudes  $s_0$  and  $w_0$  are related by the module  $m$  and parameter  $\lambda_c$  as follows

$$s_0 + w_0 = \pi m \quad (5)$$

$$\lambda_c = \frac{s_0}{w_0} \quad (6)$$

Parameter  $\lambda_c$  may be varied for optimization, in conventionally design  $\lambda_c = 1$ .

The rack-cutter surface parameters  $(u_i, l_i)$  ( $i = 1, s$ ) are measured in profile and longitudinal directions, respectively.

The rack-cutter surface  $\Sigma_c$  is represented in coordinate system  $S_c$  by vector function  $\mathbf{r}_c(u_i, l_i)$  that yields

$$\begin{aligned} x_c(u_i, l_i) &= \frac{s_0}{2} \cos \alpha_n \sin \alpha_n + u_i \cos \alpha_n \\ y_c(u_i, l_i) &= \left( \frac{s_0}{2} \cos^2 \alpha_n - u_i \sin \alpha_n \right) \cos \beta - l_i \sin \beta \\ z_c(u_i, l_i) &= \left( \frac{s_0}{2} \cos^2 \alpha_n - u_i \sin \alpha_n \right) \sin \beta - l_i \cos \beta \end{aligned} \quad (7)$$

The unit normal to  $\Sigma_c$  is determined as

$$\mathbf{n}_c^{(i)} = [\sin \alpha_n \quad \cos \alpha_n \cos \beta \quad \cos \alpha_n \sin \beta]^T \quad (8)$$

The coordinate systems applied for derivation of pinion and shaper surfaces are (fig. 5(c)):

- (i) movable coordinate systems  $S_c$  and  $S_i$  rigidly connected to the rack-cutter and the pinion (shaper),
- (ii) fixed one  $S_a$ .

The rack-cutter and the pinion (shaper) perform related motions



$$s_c = \Psi_i r_{pi} \quad (i = 1, s) \quad (9)$$

where  $r_{pi}$  is the radius of the pitch circle of the pinion (shaper).

Surface  $\Sigma_i$  ( $i = 1, s$ ) is derived as the envelope to the family of surfaces  $\Sigma_c$  represented in  $S_i$  ( $i = 1, s$ ) and is determined by the equations

$$r_i(u_i, l_i, \Psi_i) = M_{ic}(\Psi_i) r_c(u_i, l_i) \quad (i = 1, s) \quad (10)$$

$$f_{ci}(u_i, l_i, \Psi_i) = n_c \cdot v_c^{(ci)} = 0 \quad (i = 1, s) \quad (11)$$

Here: vector function  $r_i(u_i, l_i, \Psi_i)$  represents the family of rack-cutter surfaces;  $f_{ci} = 0$  is the equation of meshing; matrix  $M_{ic}(\Psi_i)$  ( $i = 1, s$ ) is applied for coordinate transformation; vector  $v_c^{(ci)}$  of the relative velocity and unit normal  $n_c$  are represented in  $S_c$ .

Vector function  $r_i(u_i, l_i, \Psi_i)$  and  $f_{ci} = 0$  represent surface  $\Sigma_i$  ( $i = 1, s$ ) by three related parameters.

Two-parameter representation of  $\Sigma_i$  ( $i = 1, s$ ) is obtained taking into account that  $f_{ci} = 0$  yields that

$$\Psi_i(u_i, l_i) = \left( \frac{\cos \beta}{r_{pi} \sin \alpha_n} \right) u_i + \left( \frac{\sin \beta}{r_{pi}} \right) l_i \quad (i = 1, s) \quad (12)$$

Then we may represent  $\Sigma_i$  as

$$R_i(u_i, l_i) = r_i(u_i, l_i, \Psi_i(u_i, l_i)) \quad (i = 1, s) \quad (13)$$

The normal to  $\Sigma_i$  is determined as

$$N_i(u_i, l_i) = \frac{\partial R_i}{\partial u_i} \times \frac{\partial R_i}{\partial l_i} \quad (14)$$

Figure 6(a) shows the solid model of the shaper. The edge of the shaper is rounded (fig. 6(b)) to generate a fillet of the face-gear with reduced bending stresses.

### 3. Generation of Face-Gear by Shaper

The tooth surface  $\Sigma_2$  of the face-gear is generated as the envelope to the family of tooth surfaces  $\Sigma_s$  of the shaper. Surface  $\Sigma_s$  of the shaper is a screw involute surface represented by equations (3) or (13) taking in these equations  $i = s$ . The surface normal to the  $\Sigma_s$  is represented by cross-products (4) or (14).

**Applied Coordinate Systems.**—We apply for the derivations the fixed coordinate systems  $S_m$  and  $S_a$  (fig. 7(a)) and movable coordinate systems  $S_2$  and  $S_m$  (fig. 7(b)). Parameter  $L_0$  for distance  $|\overline{O_2 O_a}|$  is chosen initially arbitrarily. Parameters  $L_2$  and  $L_1$  determine the outer and inner dimensions of the face gear and can be obtained from the conditions of avoidance of undercutting and pointing (see below).

Angle  $\gamma_m$  is formed by the axes of the face-gear and the shaper. Parameter  $r_{ps}$  is the radius of the pitch cylinder of the shaper. Parameter  $a_f$  is the addendum of the face-gear. The shaper and the face-gear perform related rotations about the  $z_a$  and  $z_m$  axes. Here,

$$\frac{\Psi_s}{\Psi_2} = \frac{N_2}{N_s} \quad (15)$$

where  $N_s$  and  $N_2$  are the numbers of teeth of the shaper and the face gear, respectively.

**Derivation of Surface  $\Sigma_2$  of the Face-Gear.**—Surface  $\Sigma_2$  is determined by the following equations:

$$\mathbf{r}_2(u_s, l_s, \Psi_s) = M_{2s}(\Psi_s) \mathbf{r}_s(u_s, l_s) \quad (16)$$

$$\left( \frac{\partial \mathbf{r}_2}{\partial u_s} \times \frac{\partial \mathbf{r}_2}{\partial l_s} \right) \cdot \frac{\partial \mathbf{r}_2}{\partial \Psi_s} = f_{s2}(u_s, l_s, \Psi_s) = 0 \quad (17)$$

Vector function  $\mathbf{r}_2(u_s, l_s, \Psi_s)$  represents in coordinate system  $S_2$  the family of shaper surfaces  $\Sigma_s$ .

Equation  $f_{s2} = 0$  is the equation of meshing. Equations (16) and (17) considered simultaneously represent the tooth surface  $\Sigma_2$  by three related parameters. The equation of meshing  $f_{s2} = 0$  may be determined as well as

$$\mathbf{N}_s \cdot \mathbf{v}_s^{(s2)} = f_{s2}(u_s, l_s, \Psi_s) = 0 \quad (18)$$

Here,  $\mathbf{N}_s$  is the normal to  $\Sigma_s$  represented in  $S_s$  and  $\mathbf{v}_s^{(s2)}$  is the relative velocity represented in  $S_s$ .

**Structure of Face-Gear Tooth.**—The tooth surface of the shaper is formed by a screw involute surface and a rounded top surface (fig. 8(a)). The tooth surfaces of the face-gear (fig. 8(b)) are formed: (i) as the working part (generated by the screw involute surface of the shaper), and (ii) as the fillet part (generated by rounded top of the shaper tooth).

Lines  $L_{s2}$  on the working part of the face-gear tooth are the lines of the instantaneous contact of the shaper and face-gear tooth surface. The length of the face-gear teeth has to be limited by dimensions  $L_1$  and  $L_2$  (fig. 7) to avoid undercutting in plane  $A$  and pointing in the plane  $B$  (fig. 8).

**Avoidance of Singularities.**—Avoidance of undercutting is based on the following ideas [7, 8]:

1. Appearance of singular points on the generated surface  $\Sigma_2$  is a warning that the surface will be undercut in the process of generation.
2. Singular points on surface  $\Sigma_2$  are generated by regular points of the generating surface  $\Sigma_s$  when the velocity of a contact point in its motion over  $\Sigma_2$  becomes zero.

$$\mathbf{v}_r^{(2)} = \mathbf{v}_r^{(s)} + \mathbf{v}^{(s2)} = 0 \quad (19)$$

3. Equation (19) and differential equation of meshing

$$\frac{d}{dt} [f_{s2}(u_s, l_s, \Psi_s)] = 0 \quad (20)$$

produces a system of four linear equations in two unknowns. The system has a certain solution for the unknowns if the matrix

$$A = \begin{bmatrix} \frac{\partial r_s}{\partial u_s} & \frac{\partial r_s}{\partial l_s} & -v_s^{(s2)} \\ \frac{\partial f_{s2}}{\partial u_s} & \frac{\partial f_{s2}}{\partial l_s} & -\frac{\partial f_{s2}}{\partial \psi_s} \frac{d\psi_s}{dt} \end{bmatrix} \quad (21)$$

has the rank  $r = 2$ . From this the following equation is obtained:

$$F_{s2}(u_s, l_s, \psi_s) = 0 \quad (22)$$

Equation of meshing (18) and equation (22) allows line  $L_s$  to be obtained on surface  $\Sigma_s$  (fig. 9) that generates singular points on  $\Sigma_2$ .

Limitation of surface  $\Sigma_s$  by line  $L_s$  (fig. 9) avoids the appearance of singular points on  $\Sigma_2$ .

Pointing of the face-gear means that the width of the top-land becomes equal to zero. The maximal value of  $L_2$  is obtained from the conditions of intersection of surfaces of opposite sides of a tooth of the face gear. The tooth length of the face-gear may be represented by a unitless coefficient  $c$  determined as:

$$c = \frac{L_2 - L_1}{m} = (L_2 - L_1) P_d \quad (23)$$

where  $m$  and  $P_d$  are the module and the diametral pitch of the shaper. The coefficient  $c$  depends on the gear ratio  $m_{12}$  and the helix angle of the shaper. Graphs shown in figure 10 are obtained for the case of the shaper helix angle  $\beta = 5^\circ$ . Input data are listed in table 1.

Comparison of a face-gear and a spiral bevel gear drives shows that a substantial larger gear ratio (up to  $m_{12} = 10$ ) and a larger tooth length can be obtained by application of a face-gear drive instead of a spiral bevel gear drive. However, the design of a face-gear drive is accompanied with the dimensions of the drive measured in directions of  $L_1$  and  $L_2$  (fig. 7(a)).

## 4. Design of Generating Worm

In the previous design, the generation of the face-gear by a grinding or cutting worm (instead of a shaper) was limited to the case wherein the driving member of the gear drive is an involute spur pinion.

Application of a helical involute pinion (instead of a spur pinion) has required a new approach for the design of the generating worm and the generation by the worm of the face-gear. Particularly, it has required: (i) the development of a two-parameter enveloping process of generation of the face-gear by the worm; (ii) investigation of limitations of generation of the face-gear caused by the magnitude of the helix angle of the shaper and the diameter of the worm.

This section of the paper covers the solution to the following problems:

1. Determination of the crossing angle between the axes of the shaper and the worm.
2. Determination of worm thread surface.
3. Avoidance of singularities of the worm thread surface.
4. Numerical examples.

**Crossing Angle Between the Axes of the Shaper and the Worm.**—The derivation of the crossing angle between the axes of the shaper and the worm and other following derivations are based on the idea of simultaneous meshing of surfaces  $\Sigma_s$ ,  $\Sigma_w$ , and  $\Sigma_2$  of the shaper, the worm, and the face-gear.

Figure 11 shows schematically that surfaces  $\Sigma_s$ ,  $\Sigma_w$ , and  $\Sigma_2$  are in tangency at point  $P$ , that is the common point of pitch surfaces of the shaper and the face-gear.

The shortest distance  $E_{ws}$  between the worm and the shaper is obtained as

$$E_{ws} = r_{pw} - r_{ps} \quad (24)$$

where  $r_{pw}$  and  $r_{ps}$  are the radii of the pitch surfaces of the worm and the shaper, respectively. The

magnitude of  $E_{ws}$  affects the dimensions of the grinding worm and the conditions of avoidance of surface singularities of the worm (see below).

The derivation of the crossing angle  $\gamma_{ws}$  between the axes of the shaper and the worm is based on the drawings of figure 12. We apply for derivations fixed coordinate systems  $S_a$ ,  $S_b$ , and  $S_c$  (fig. 12) and movable coordinate systems  $S_s$  and  $S_w$  rigidly connected to the shaper and the worm, respectively.

Figure 13 in addition to figure 11 illustrates that the pitch cylinders of the worm and the shaper are in tangency at point  $P$ . Angles  $\lambda_w$  and  $\beta$  represent the lead angle of the worm and the helix angle of the shaper. The shaper is considered as a left-hand involute helicoid. Figure 13 illustrates the tangency with the left-hand shaper of a right hand-worm (fig. 13(a)) and a left hand-worm (fig. 13(b)). The shaper and the worm perform rotations about the axes  $z_a$  and  $z_c$ . The angles of rotation of the shaper and the worm are designated by  $\psi_s$  and  $\psi_w$  (fig. 12).

The velocity polygons at point of tangency  $P$  are represented in figure 13. Vectors  $v^{(s)}$  and  $v^{(w)}$  are the velocities of the shaper and the worm at point  $P$ . The sliding velocity at point  $P$  is designated as  $v^{(sw)} = v^{(s)} - v^{(w)}$ . Vector  $i_t$  is the unit vector of the tangent to the helices of the shaper and the worm.

Taking into account that the sliding velocity  $v^{(sw)}$  is collinear to vector  $i_t$  we obtain the following relations

$$\gamma_{ws} = 90^\circ - \beta \pm \lambda_w \quad (25)$$

$$\lambda_w = \arcsin \frac{r_{ps} N_w \cos \beta}{N_s (E_{ws} + r_{ps})} \quad (26)$$

Here:  $N_s$  and  $N_w$  are the tooth numbers of the shaper and the threads of the worm. The upper and lower signs in equation (25) correspond to the application of a right-hand worm and left-hand worm, respectively.

**Derivation of Worm Thread Surface  $\Sigma_w$ .**—The worm thread surface  $\Sigma_w$  is determined as an envelope to the family of shaper tooth surfaces  $\Sigma_s$ .

Surface  $\Sigma_w$  is determined in coordinate system  $S_w$  by the following equations

$$r_w(u_s, l_s, \psi_s) = M_{ws}(\psi_s) r_s(u_s, l_s) \quad (27)$$

$$N_s \cdot v_s^{(sw)} = f_{ws}(u_s, l_s, \psi_s) = 0 \quad (28)$$

Here: vector function  $\mathbf{r}_s(u_s, l_s)$  represents the tooth surface of the shaper. Matrix  $\mathbf{M}_{ws}(\psi_s)$  describes the coordinate transformation from coordinate system  $S_s$  to coordinate system  $S_w$  (fig. 12). Vector function  $\mathbf{r}_w(u_s, l_s, \psi_s)$  represents in coordinate system  $S_w$  the family of surfaces  $\Sigma_s$  of the shaper. Equation (28) is the equation of meshing between the surfaces of the shaper and the worm. Parameter  $\psi_s$  is the generalized parameter of motion considering that the shaper and the worm perform related rotations about the axes  $z_a$  and  $z_c$  (fig. 12). These rotations are related by the equation

$$\frac{\Psi_s}{\Psi_w} = \frac{N_w}{N_s} \quad (29)$$

where  $N_s$  and  $N_w$  are the number of teeth of shaper and the number of threads of the worm. Equations (27) and (28) considered together represent the worm thread surface by three related parameters  $(u_s, l_s, \psi_s)$ .

We may represent the worm thread surface in two-parameter form by using the theorem of implicit function system existence [6]. Assume that point  $M(u_s^{(0)}, l_s^{(0)}, \psi_s^{(0)})$  satisfies the equation of meshing  $f_{ws} = 0$  (see equation (28)) and at point  $M$  we have that  $\frac{\partial f_{ws}}{\partial l_s} \neq 0$ .

Then, equation of meshing (28) may be solved in the neighborhood of  $M$  by a function of class  $C^1$  as

$$l_s = l_s(u_s, \psi_s) \quad (30)$$

and the worm thread surface may be determined locally, in the neighborhood of  $M$ , as

$$\mathbf{R}_w(u_s, \psi_s) = \mathbf{r}_w(u_s, l_s(u_s, \psi_s), \psi_s) \quad (31)$$

**Singularities of Worm Thread Surface.**—The main difficulty of application of the worm as a tool for the generation of the face-gear tooth surface is the possibility of appearance of singularities on the worm thread surface  $\Sigma_w$ .

The existence of singularities of surface  $\Sigma_w$  may require to limit the magnitude of the helix angle of the shaper (and the pinion too) and require as well to limit the diameter of the worm.

Avoidance of worm singularities is the precondition to application of the worm for generation of the face-gear.

The discovery of worm singularities is based on the approach [8] discussed previously in section 3 for avoidance of singularities of the face-gear that is generated by a shaper.

A similar approach for determination of singularities of the worm surface  $\Sigma_w$  (determined as the envelope to the family of shaper tooth surface  $\Sigma_s$ ) is based on the following considerations:

1. The equation of meshing of the worm and the shaper is determined as (see equation (28))

$$f_{ws}(u_s, l_s, \psi_s) = 0 \quad (32)$$

2. The differentiated equation of meshing is represented as

$$\frac{d}{dt}[f_{ws}(u_s, l_s, \psi_s)] = 0 \quad (33)$$

3. Singularities on the worm surface occur at a point where the velocity  $v_r^{(w)}$  of the contact point in its motion over the worm surface  $\Sigma_w$  becomes equal to zero. The condition  $v_r^{(w)} = 0$  yields the relation [8]

$$v_r^{(s)} + v^{(sw)} = 0 \quad (34)$$

Here:  $v_r^{(s)}$  is the velocity of the contact point in its motion over the shaper surface, and  $v^{(sw)}$  is the velocity of sliding in the process of meshing of surfaces  $\Sigma_s$  and  $\Sigma_w$ .

4. Application of equations (33) and (34) yields a system of four linear equations in two unknowns. The system of four linear equations has a certain solution for the unknowns if the matrix

$$A = \begin{bmatrix} \frac{\partial r_s}{\partial u_s} & \frac{\partial r_s}{\partial l_s} & -v_s^{(sw)} \\ \frac{\partial f_{ws}}{\partial u_s} & \frac{\partial f_{ws}}{\partial l_s} & -\frac{\partial f_{ws}}{\partial \psi_s} \frac{d\psi_s}{dt} \end{bmatrix} \quad (35)$$

has the rank  $r = 2$ .

The requirement  $r = 2$  results in the following equation:

$$F_{ws}(u_s, l_s, \psi_s) = 0 \quad (36)$$

The simultaneous consideration of equation of meshing  $f_{ws} = 0$  (see equation (28)) and equation  $F_{ws} = 0$  (see equation (36)) is the key for design of a worm free of singularities.

**Illustration of Simultaneous Meshing of Surfaces  $\Sigma_w$ ,  $\Sigma_s$ , and  $\Sigma_2$ .**—A worm (free of singularities) may be in simultaneous meshing with the shaper and the face-gear as it is illustrated in figure 14. Separate meshing of the shaper with the face-gear, and the worm with the face-gear, are represented in figure 15.

It will be shown below that avoidance of worm singularities can be achieved by limitation of the helix angle of the shaper (simultaneously, the pinion) and the decrease of the diameter of the worm.

Usually, the diameter of the worm is chosen larger than the shaper diameter, but this may require to decrease the shaper helix angle for avoidance of singularities.

Figure 16 shows application of a worm which diameter is chosen less than the diameter of the shaper for the purpose of the increase of the helix angle of the shaper (and the pinion). Separate meshing of the shaper with the face-gear, and the worm with the face-gear, are represented in figure 17.

A generating worm of a lesser diameter can be applied as a hob or as a shaving worm.

**Avoidance of Worm Singularities.**—Singularities of the worm are avoided as follows.

Using the equation of meshing between the worm and the shaper, we may represent the lines of tangency of  $\Sigma_w$  and  $\Sigma_s$  in the plane of surface parameters  $(u_s, l_s)$ . The lines of tangency of  $\Sigma_w$  and  $\Sigma_s$  are given in two examples. The common data for these two examples are shown in table 2.

Example 1: A left-hand shaper is in mesh with a right-hand worm. The helix angle of the shaper is  $5^\circ$ . Figures 18(a) and (b) show the contact lines and undercutting lines on the drive and coast sides, respectively.

Singularities of the worm may be avoided if the angle of rotation of the worm is in the area of contact lines that do not intersect the undercutting lines.

Such area has to be determined taking into account that the driving and coast sides of the tooth are generated simultaneously.

Graphs of figures 18(a) and (b) show that the maximal permissible rotation angle of the shaper should not exceed the angle  $\psi_s < |7.63^\circ| + |-7.63^\circ| = 15.26^\circ$ . The angle of rotation of the shaper for one cycle of meshing is

$$\psi_s = \frac{360^\circ}{N_s} = 12^\circ \quad (N_s = 30) \quad (37)$$

Singularities are avoided if the angle of rotation of the shaper does not exceed  $15.26^\circ$ .

Example 2: The helix angle of the shaper is  $15^\circ$  and the diameter of the worm is smaller than the diameter of the shaper (figs. 16 and 17). Other conditions are the same as in example 1 (see table 2).

Unlike example 1, we have found in example 2 that there is an envelope  $E$  to the family of contact lines in the working area (fig. 19). The envelope is determined (see [9, 11]) by the equation of meshing

$$f_{sw}(u_s, l_s, \psi_s) = 0 \quad (38)$$

and the derivative

$$\frac{\partial f_{sw}}{\partial \psi_s} = 0 \quad (39)$$

Due to the existing of envelope  $E$  to the contact lines, the determination of worm surface  $\Sigma_w$  as the envelope to the family of shaper surfaces requires interpretation of formation of  $\Sigma_w$  by two branches differentiated by  $\frac{\partial f_{sw}}{\partial \psi_s} > 0$  and  $\frac{\partial f_{sw}}{\partial \psi_s} < 0$ .

Singularities of the worm in example 2 are avoided if the maximal angle of rotation of the shaper for one cycle of meshing will satisfy the inequality (fig. 19).

$$\frac{360^\circ}{N_s} < |6.15^\circ| + |-6.15^\circ| \quad (40)$$

Using computations similar to the examples discussed above, we may represent a graph (fig. 20) that illustrates the permissible helix angle of the shaper as the function of the ratio of radii  $\frac{r_{pw}}{r_{ps}}$  of the pitch cylinders of the worm and the shaper.

## 5. Generation of Face-Gear by Worm

Traditionally, the generation of a face-gear that is conjugated to a spur involute pinion is performed by a shaper.

Application of a worm for generation of face-gears [10] opens the possibility of grinding, hobbing, and shaving. In case of hobbing, the worm is designed as a hob.

The design of face-gear drives in the past was limited to application of a spur pinion as a driving member. Application of a helical pinion requires a new approach for the generation of a face-gear by a worm.

Considering the simultaneous meshing of a worm, shaper, and face-gear (figs. 14 and 16), we have to take into account the following:

The shaper surface  $\Sigma_s$  is in line contact with the face-gear tooth surface  $\Sigma_2$  and with the worm surface  $\Sigma_w$  as well. Designations  $L_{s2}$  and  $L_{sw}$  indicate the lines of tangency of surfaces  $\Sigma_s$  and  $\Sigma_2$  and of tangency of  $\Sigma_s$  and  $\Sigma_w$  (figs. 21(a) and (b)). However, the worm and the face-gear surfaces  $\Sigma_w$  and  $\Sigma_2$  are in point contact at every instant since contact lines  $L_{s2}$  and  $L_{sw}$  do not coincide but intersect each with other (fig. 21(c)).

Consider now that the worm and the face-gear perform rotations about their axes related by equation

$$\frac{\Psi_w}{\Psi_2} = \frac{N_2}{N_w} \quad (41)$$

Here:  $N_2$  and  $N_w$  are the number of teeth of the face-gear and the number of threads of the worm.

Usually,  $N_w = 1$  since a one-thread worm is applied.

Due to point tangency of surfaces  $\Sigma_w$  and  $\Sigma_2$ , the worm will generate on surface  $\Sigma_2$  only a strip.

The generation by the worm of the whole surface  $\Sigma_2$  (instead of a strip) requires application of two-parameter enveloping process that is based on the following ideas:

1. Consider that the worm, the shaper, and the face-gear are in simultaneous meshing (fig. 14). The worm and the face-gear perform rotations related by equation (41), but the worm generates a strip on the face-gear.
2. The whole surface of the face-gear may be generated as a set of strips, but this requires a feed motion of the worm with respect to the face-gear. The feed motion means that the installment of the worm with respect to the face-gear has to be varied in the process of generation. The worm will generate at each installment a strip on the face-gear tooth surface. In the following discussions, we initially interpret the feed motion as a discrete process.
3. A new installment of the worm, the shaper, and the face-gear are performed as follows:
  - The worm is translated in the direction of the axis of the shaper on  $\Delta l_w$  and, simultaneously, the shaper is turned on angle  $\Delta \psi_s$  (fig. 22). The magnitudes of  $\Delta l_w$  and  $\Delta \psi_s$  are components of screw motion of the worm about the axis of the shaper related as

$$\frac{\Delta l_w}{\Delta \psi_s} = p_s \quad (42)$$

Here,  $p_s$  is the screw parameter of the shaper.

Observation of equation (42) provides tangency of  $\Sigma_w$  and  $\Sigma_s$  at each installment.

- Simultaneous tangency of three surfaces at each installment requires that the face-gear will be turned angle  $\Delta \psi_2$  determined as

$$\Delta \psi_2 = \Delta \psi_s \frac{N_s}{N_2} = \frac{\Delta l_w}{p_s} \frac{N_s}{N_2} \quad (43)$$



4. The derivation of the face-gear tooth surface generated by the worm may be now represented as a continuous two-parameter enveloping process based on application of two independent sets of parameters:
- set one formed by  $(\psi_w, \psi_2)$  related by equation (41), and
  - set two of parameters  $(\Delta l_w, \Delta \psi_2)$  related by equation (43)

Surface  $\Sigma_2$  of face-gear generated by the worm is determined as the envelope to the two-parameter family of surfaces of worm thread surface as follows [8, 16]:

$$r_2(u_s, \psi_s, \psi_w, \Delta l_w) = M_{2w}(\psi_w, \Delta l_w) R_w(u_s, \psi_s) \quad (44)$$

$$N_w \cdot v_w^{(w2, \psi_w)} = f_{w2}^{(1)}(u_s, \psi_s, \psi_w, \Delta l_w) = 0 \quad (45)$$

$$N_w \cdot v_w^{(w2, \Delta l_w)} = f_{w2}^{(2)}(u_s, \psi_s, \psi_w, \Delta l_w) = 0 \quad (46)$$

Here, vector function  $r_2(u_s, \psi_s, \psi_w, \Delta l_w)$  represents in coordinate system  $S_2$  the family of thread worm surfaces. Equations (45) and (46) are the two equations of meshing.  $u_s, \psi_s$  are the worm surface parameters. Generalized independent parameters of motion are designated as  $\psi_w$  and  $\Delta l_w$  and the two independent sets of parameters are:  $(\psi_w, \psi_2)$  and  $(\Delta l_w, \Delta \psi_2)$ .  $N_w$  is the normal to the worm surface at the current point of contact and is represented in system  $S_w$ . Vector  $v_w^{(w2, \psi_w)}$  represents the relative sliding velocity between the worm and the face-gear determined under the condition that generalized parameter  $\psi_w$  of motion is varied and the other generalized parameter  $\Delta l_w$  is held to the rest. Similarly, vector  $v_w^{(w2, \Delta l_w)}$  represents the relative sliding velocity between the worm and the face-gear but it is determined under the condition that the parameter  $\Delta l_w$  is varied and the other generalized parameter of motion  $\psi_w$  is held at rest. Both vectors of relative velocity are represented in system  $S_w$ . Vector equations (44), (45), and (46), if considered simultaneously, determine surface  $\Sigma_2$  as the envelope of two-parameter enveloping process. Applied coordinate systems are shown in figure 22.

Vector function  $r_2(u_s, \psi_s, \psi_w, \Delta l_w)$  and equations of meshing  $f_{w2}^{(1)} = 0$  and  $f_{w2}^{(2)} = 0$  represent surface  $\Sigma_2$  generated by the worm by four related parameters.

The analysis results of face-gear tooth surface  $\Sigma_2$  are illustrated in figure 23 by: (a) cross-sections of  $\Sigma_2$ , and (b) strip lines on  $\Sigma_2$ .

The computations have been performed for determination of surface  $\Sigma_2$  twice, wherein  $\Sigma_2$  is generated by a shaper and by a worm. Comparison of obtained results confirms the identity of the surfaces.

## 6. Tooth Contact Analysis (TCA)

TCA is designated for simulation of meshing and contact of surfaces  $\Sigma_1$  and  $\Sigma_2$  of helical pinion and face-gear and permits the influence of errors of alignment on transmission errors and shift of bearing contact to be investigated. The TCA algorithm is based on observation of continuous tangency of pinion and face-gear tooth surfaces  $\Sigma_1$  and  $\Sigma_2$  in the process of meshing. Application of TCA shows: (i) errors of alignment do not cause transmission errors but (ii) cause the shift of the bearing contact.

The TCA computer program is based on the following algorithm:

1. The helical pinion surface  $\Sigma_1$  and its surface unit normal are represented in coordinate systems  $S_1$  by the following vector functions

$$\mathbf{r}_1(u_1, l_1) \quad , \quad \mathbf{n}_1(u_1, l_1) \quad (47)$$

Similarly, the face-gear surface  $\Sigma_2$  and its surface unit normal are represented in  $S_2$  by vector functions

$$\mathbf{r}_2(u_s, l_s, \psi_s) \quad , \quad \mathbf{n}_2(u_s, l_s, \psi_s) \quad (48)$$

and equation of meshing between the shaper and the face-gear

$$f_{s2}(u_s, l_s, \psi_s) = 0 \quad (49)$$

2. Using coordinate transformation, we represent the conditions of continuous tangency of  $\Sigma_1$  and  $\Sigma_2$  in a fixed coordinate system  $S_f$  as

$$\mathbf{r}_f^{(1)}(u_1, l_1, \phi_1) - \mathbf{r}_f^{(2)}(u_s, l_s, \psi_s, \phi_2) = 0 \quad (50)$$

$$\mathbf{n}_f^{(1)}(u_1, l_1, \phi_1) - \mathbf{n}_f^{(2)}(u_s, l_s, \psi_s, \phi_2) = 0 \quad (51)$$

$$f_{s2}(u_s, l_s, \psi_s) = 0 \quad (52)$$

3. The system of nonlinear equations (50) to (52) contains only six independent nonlinear scalar equations in seven unknowns since  $|\mathbf{n}_f^{(1)}| = |\mathbf{n}_f^{(2)}| = 1$ .

One of the parameters, say  $\phi_1$ , is chosen as the input parameter. The solution of equations mentioned above is represented by functions of  $\phi_1$ , and it is a computerized iterative process based on the Newton-Raphson method [6]. Surfaces  $\Sigma_1$  and  $\Sigma_2$  are in point tangency and the Jacobian of the system of equations of tangency differs from zero.

We apply for derivation of the equations (50) to (52) and the performance of TCA the following coordinate systems: movable coordinate systems  $S_1$  and  $S_2$  rigidly connected to the helical pinion and the face-gear (figs. 24(a) and (d)); main fixed coordinate system  $S_f$  rigidly connected to the frame where the meshing of the pinion and the gear is considered (figs. 24(a) and (b)); auxiliary fixed coordinate systems  $S_a$ ,  $S_b$ , and  $S_c$  (figs. 24(b), (c), and (d)) applied for simulation of errors of installment  $\Delta\gamma_m$ ,  $\Delta E$ , and  $\Delta q$  (figs. 24(b) and (c)).

Figure 25 in addition to figure 24 illustrates the installment of coordinate systems  $S_a$ ,  $S_b$ , and  $S_c$  with respect to  $S_f$  that is represented in an axial section of the face-gear taking error  $\Delta E$  equal to zero. Here, magnitude  $B$  is given by

$$B = \frac{m N_s - N_1}{2 \cos \beta} \quad (53)$$

The simulation of meshing is performed for two cases of face-gear drives: with a helical involute pinion and a spur involute pinion with design parameters represented in table 3.

The output of the TCA shows that errors of installment do not cause transmission errors, but the bearing contact is shifted due to misalignment. Figure 26 illustrates the paths of contact for an aligned gear drive: (a) with a helical pinion; (b) with a spur pinion.

Figure 27 illustrates the shift of the bearing contact due to errors  $\Delta\gamma_m$  and  $\Delta E$ . It was discovered that the shift of bearing contact caused by errors of alignment  $\Delta\gamma_m$  and  $\Delta E$  may be restored by correction  $\Delta q$  (see figs. 24 and 25 that illustrate  $\Delta q$ ). Figure 28 illustrates results of application of correction  $\Delta q$  for compensation of errors  $\Delta\gamma_m$ ,  $\Delta E$ , and for simultaneous existence of  $\Delta\gamma_m$  and  $\Delta E$ .

## 7. Stress Analysis

The goals of stress analysis represented in this section are:

1. Determination of contact and bending stresses and investigation of formation of the bearing contact in a face-gear drive with a helical involute pinion.
2. Comparison of contact and bending stresses for a face-gear drive with a helical involute pinion to a face-gear drive with a spur involute pinion.

The stress analysis performed is based on finite element method [26] and application of a general computer program [5].

The approach developed for the finite element models is accomplished as follows:

Step 1. Tooth surface equations of pinion and face gear and portions of corresponding rim are considered for determination of the volumes of the designed bodies. Figure 29(a) shows the designed body for one-tooth model of the pinion of a face-gear drive.

Step 2. The designed volume of each tooth of the model is divided into six subvolumes using auxiliary intermediate surfaces 1 to 6 as shown in figure 29(b).

Step 3. Node coordinates are determined analytically considering the number of desired elements in longitudinal and profile directions (fig. 29(c)).

Step 4. Discretization of the model by finite elements is accomplished using the nodes determined in previous step (fig. 29(d)).

Step 5. Setting of boundary conditions is accomplished on pinion and face-gear models considering the following ideas (see fig. 30 for the case of a three-tooth model):

- Nodes on the two sides and bottom part of the portion of the face-gear rim are considered as fixed (fig. 30(a)).
- Nodes on the two sides and the bottom part of the pinion rim form a rigid surface (figs. 30(a) and (b)).
- A reference node  $N$ , (fig. 30(b)) located in the axis of the pinion is used as the reference point of the previous defined rigid surface. Reference point  $N$  and the rigid surface constitute a rigid body.
- Only one degree of freedom is defined as free at the reference point  $N$ , rotation about the pinion axis, while all other degrees of freedom are fixed. Application of a torque  $T$  in rotational motion at the reference point  $N$  allows us to apply such a torque to the pinion model.

Step 6. The contact algorithm of the finite element analysis computer program requires definition of contacting surfaces. This approach enables us to identify automatically all the elements of the model required for the formation of such surfaces.

Figures 31(a) and (b) show the finite element models of one-tooth of the pinion and the face gear. The development of the finite element model of the face gear is complicated due to the specific structure of the face gear tooth (see fig. 8(b)). While in the pinion model the profile and fillet parts can be meshed independently, in the face-gear model both parts have to be considered simultaneously.

The principal characteristics of the described approach are as follows:

- Finite element models of the face gear drive can be automatically obtained for any position of pinion and face gear obtained from TCA. Stress convergence is assured because there is at least one point of contact between the contacting surfaces.
- Assumption of load distribution in the contact area are not required since the contact algorithm of the general computer program is used to find the contact area and stresses by application of the torque to the pinion while the gear is considered fixed at specified surfaces (see fig. 30(a)).
- Finite element models of any number of teeth can be obtained. As an example, figure 32 shows a whole face gear drive finite element model. However, such a model is not recommended, if an exact definition of the contact ellipse is required. Three or five tooth models are more adequate in such a case. The use of several teeth in the models has the following advantages:
  - (i) Boundary conditions are far enough from the loaded areas of the teeth.
  - (ii) Simultaneous meshing of two pairs of teeth can occur due to the elasticity of surfaces.
 Therefore, the load transition at the beginning and at the end of the path of contact can be studied.

**Numerical Example.**—The finite element analysis has been performed for the following cases mentioned above:

1. Face-gear drive with helical involute pinion.
2. Face-gear drive with spur involute pinion.

The applied design parameters are shown in table 3. The output from TCA (see figs. 26(a) and (b)) and the developed approach for the finite element models allows us to build automatically one model for every point of contact.

A three teeth model has been developed for each chosen point of the path of contact. Elements C3D8I of first order (enhanced by incompatible modes to improve their bending behavior) have been used to form the finite element mesh. The total number of elements is 71,460 with 87,360 nodes. The material is steel with the properties of Young's Modulus  $E = 2.068 \cdot 10^5$  MPa and Poisson's ratio 0.29. A torque of 4,000 Nm has been applied to the pinion in both cases. Figure 33 shows the finite element mesh for case (1) in a contact point. Figures 34 and 35 show the maximum contact and bending stresses obtained at such a contact point on the pinion surface in cases (1) and (2), respectively. Figures 36 and 37 show the maximum contact and bending stresses obtained at the same contact point, but on the face gear surface in cases (1) and (2), respectively.

The variation of contact and bending stresses along the path of contact has been also studied. Figures 38 and 39 illustrate the variation of contact and bending stresses, respectively, for both cases. A reduction of contact stresses has been achieved by using a face-gear drive with a helical involute pinion in comparison with a face-gear drive with a spur involute pinion. However, an edge contact exists in both gear drives, because the path of contact is oriented across the tooth surface (see fig. 26).

The goal of avoidance of edge contact requires application of non-involute geometry of the pinion and the shaper for obtaining of a longitudinal orientation of the bearing contact, instead of orientation of the bearing contact across the tooth surfaces. The obtained bending stresses show that the stresses for gear drives with a spur and helical pinions are comparable.

## 8. Conclusions

The results of performed research allow the following conclusions to be drawn:

1. A new type of face-gear drive with intersected axes of rotation has been investigated. The gear drive is formed by an involute helical pinion and conjugated face-gear.
2. The perspectives of application of the new type of gear drive in comparison with spiral bevel gears are: (i) a higher gear ratio (up to  $m_{12} = \frac{\omega^{(1)}}{\omega^{(2)}}$  of 7); (ii) a more simple technology in comparison with spiral bevel gears and hypoid gear drives; (iii) errors of misalignment such as crossing of axes instead of intersection do not cause transmission errors; (iv) the bearing contact is localized and the shift of bearing contact caused by misalignment may be compensated.

However, application of face-gear drives of a higher gear ratio is accompanied with the increase of the face width of the gear drive measured in the direction of axes of the pinion.

3. A computerized design of gear drives has been developed that avoids singularities, simulates meshing of misaligned gear drives and permits the stress analysis to be performed. The contacting model for stress analysis is developed automatically.

The developed design determines the maximal tooth length free of pointing and undercutting and the limitations of the helix angle of the pinion for conjugation of face-gears ground by a worm.

A new method of manufacturing based on application of a grinding and cutting worm of a special shape has been developed.

## References

- [1] Argyris, J., Litvin, F.L., Lian, Q., and Lagutin, S.A., *Determination of Envelope to Family of Planar Parametric Curves and Envelope Singularities*, Computer Methods in Applied Mechanics and Engineering, vol. 175, no. 1–2, pp. 175–187, 1999.
- [2] Argyris, J., Litvin, F.L., Peng, A., and Stadtfeld, H.J., *Axes of Meshing and Their Application in Theory of Gearing*, Computer Methods in Applied Mechanics and Engineering, vol. 163, no. 1–4, pp. 293–310, 1998.
- [3] Baumann, V., Bär, G., Haase, A., Hutschenreiter, B., Hünecke, C., and Dutschk, R., *BECAL 2.0 Programm zur Berechnung der Zahnflanken und Zahnfußbeanspruchung an Kegelrad- und Hypoidgetrieben bei Berücksichtigung der Verformungen und Abweichungen der Getriebe-elemente*, FVA-Heft 548, Forschungsvereinigung Antriebstechnik, 1998.
- [4] Bär, G., *Curvatures of the Enveloped Helicoid*, Mechanism and Machine Theory, vol. 32, no. 1, pp. 111–120, 1997.
- [5] Hibbit, Karlsson & Sirensen, Inc., *ABAQUS/Standard 6.1 User's Manual*, 1800 Main Street, Pantucket, RI 02860–4847, 1998.
- [6] Korn, G.A. and Korn, T.M., *Mathematics Handbook for Scientist and Engineers*, McGraw-Hill, Inc., 2nd Ed., 1968.
- [7] Litvin, F.L., *Theory of Gearing*, NASA RP–1212 (AVSCOM 88-C–C035), Washington, D.C., 1989.
- [8] Litvin, F.L., *Gear Geometry and Applied Theory*, Prentice Hall, Inc., Englewood Cliffs, New Jersey, 1994.
- [9] Litvin, F.L., *Development of Gear Technology and Theory of Gearing*, NASA Reference Publication 1406, ARL-TR–1500, 1998.
- [10] Litvin, F.L., Chen, Y.-J., Heath, G.F., Sheth, V.J., and Chen, N., Apparatus and Method for Precision Grinding Face Gears, USA Patent 6, 146, 253, 2000.
- [11] Litvin, F.L., Demenego, A., and Vecchiato, D., *Formation by Branches of Envelope to Parametric Families of Surfaces and Curves*, Journal Computer Methods in Applied Mechanics and Engineering, vol. 190, pp. 4587–4608, 2001.
- [12] Litvin, F.L., Egelja, A.M., and De Donno, M., *Computerized Determination of Singularities and Envelopes to Family of Contact Lines on Gear Tooth Surface*, Journal Computer Methods in Applied Mechanics and Engineering, vol. 158, no. 1–2, pp. 23–34, 1998.
- [13] Litvin, F.L., Fuentes, A., Zanzi, C., Pontiggia, M., and Handschuh, R., F., *Face Gear Drive with Spur Involute Pinion: Geometry, Generation by a Worm, Stress Analysis*, Computer Methods in Applied Mechanics and Engineering, vol. 191, pp. 2785–2813, 2002.
- [14] Litvin, F.L., De Donno, M., Peng, A., Vorontsov, A., and Handschuh, R.F., *Integrated Computer Program for Simulation of Meshing and Contact of Gear Drives*, Computer Methods in Applied Mechanics and Engineering, vol. 181, no. 1–3, pp. 71–85, 2000.
- [15] Litvin, F.L., Peng, A., and Wang, A.G., *Limitation of Gear Tooth Surfaces by Envelopes to Contact Lines and Edge of Regression*, Mechanism and Machine Theory, vol. 34, no. 6, pp. 889–902, 1999.

- [16] Litvin, F.L., Seol, I.H., *Computerized determination of gear tooth surface as envelope to two parameter family of surfaces*, Computer Methods in Applied Mechanics and Engineering, vol. 138, pp. 213–225, 1996.
- [17] Litvin, F.L., Wang, J.-C., Chen, Y.-J.D., Bossler, R.B., Heath, G.F., and Lewiki, D.J., *Face-gear drives: Design, analysis and testing for helicopter transmission applications*, AGMA paper 92FTM2, 1992.
- [18] Litvin, F.L., Zhang, Y., Wang, J.-C., Bossler, R.B., Chen, Y.-J.D., *Design and geometry of face-gear drives*, ASME Journal of Mechanical Design, vol. 114, pp. 642–647, 1992.
- [19] Sheveleva, G.I., *Mathematical simulation of spiral bevel gear production and meshing processes with contact and bending stresses*, In Proc. IX World Congr. IFToMM, vol. 1, pp. 509–513, 1995.
- [20] Stadtfeld, H.J., *Handbook of Bevel and Hypoid Gears: Calculation, Manufacturing, and Optimization*, Rochester Institute of Technology, Rochester, New York, 1993.
- [21] Stosic, N., *On Gearing of Helical Screw Compressor Rotors*, Proc IMechE, Journal of Mechanical Engineering Science, vol. 212, pp. 587–594, 1998.
- [22] Stosic, N., *Recent developments in screw compressors*, Proc IMechE, Journal of Mechanical Engineering Science, C542/066, 1999.
- [23] Stosic, N. and Hanjalic, K., *Development and Optimization of Screw Machines with a Simulation Model. Part I: Profile generation*, ASME Transactions, Journal of Fluids Engineering, vol. 119, pp. 659–663, 1997.
- [24] Zalgaller, V.A., *Theory of Envelopes*, Publishing House Nauka (in russian), 1975.
- [25] Zalgaller, V.A. and Litvin, F.L., *Sufficient Condition of Existence of Envelope to Contact Lines and Edge of Regression on the Surface of the Envelope to the Parametric Family of Surfaces represented in Parametric Form*, Proceedings of Universities: Mathematics (in russian), vol.178, no. 3, pp. 20–23, 1977.
- [26] Zienkiewicz, O.C. and Taylor, R.L., *The Finite Element Method*, John Wiley & Sons, 5<sup>th</sup> Ed., 2000.

TABLE 1.—DESIGN PARAMETERS OF FACE GEAR DRIVE SHOWN IN FIGURE 10

Number of teeth of the face gear, $N_2$	140
Number of teeth of the worm, $N_w$	1
Module, $m$	3.175 mm
Normal pressure angle, $\alpha_n$	27.5°
Parameter of rack-cutter, $\lambda_c$	1
Shaft angle, $\gamma_m$	90.0°
Helix angle, $\beta$	5.0°
Inner radius of the face gear, $L_1$	205.0 mm
Outer radius of the face gear, $L_2$	248.0 mm

TABLE 2.—DESIGN PARAMETERS OF THE WORM

Number of teeth of the shaper, $N_s$	30
Number of teeth of the face gear, $N_2$	140
Number of threads of the worm, $N_w$	1
Module, $m$	3.175 mm
Normal pressure angle, $\alpha_n$	27.5°
Parameter of rack-cutter, $\lambda_c$	0.95

TABLE 3.—DESIGN PARAMETERS OF FACE-GEAR DRIVE

Number of teeth of the pinion, $N_1$	25
Number of teeth of the shaper, $N_s$	28
Number of teeth of the face gear, $N_2$	160
Module, $m$	6.35 mm
Normal pressure angle, $\alpha_n$	25.0°
Parameter of rack-cutter, $\lambda_c$	0.9
Shaft angle, $\gamma_m$	90.0°
Helix angle <sup>(1)</sup> , $\beta$	15.0°
Inner radius of the face gear <sup>(1)</sup> , $L_1$	500.0 mm
Outer radius of the face gear <sup>(1)</sup> , $L_2$	590.0 mm
Helix angle <sup>(2)</sup> , $\beta$	0.0°
Inner radius of the face gear <sup>(2)</sup> , $L_1$	480.0 mm
Outer radius of the face gear <sup>(2)</sup> , $L_2$	570.0 mm

<sup>(1)</sup> Face-gear drive with helical involute pinion

<sup>(2)</sup> Face-gear drive with spur involute pinion

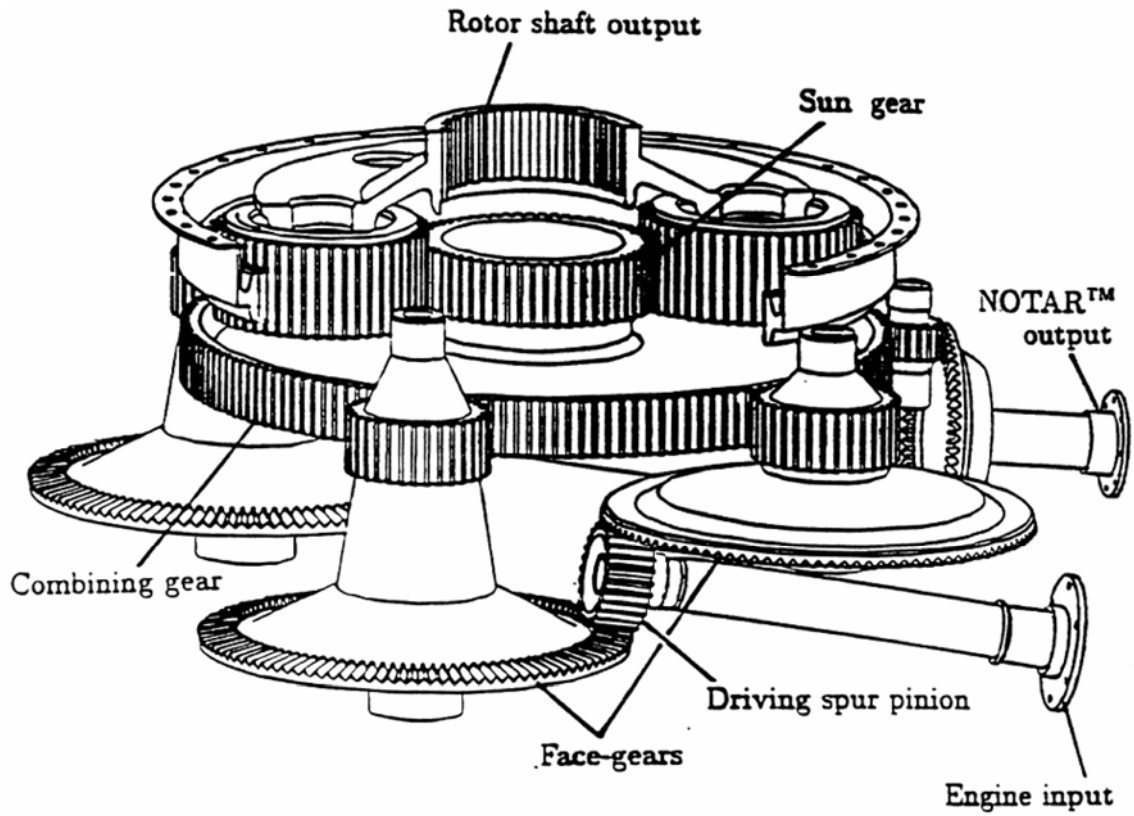


Figure 1.—Application of face-gear drive in helicopter transmission.



Figure 2.—Face-gear drive with a helical pinion.



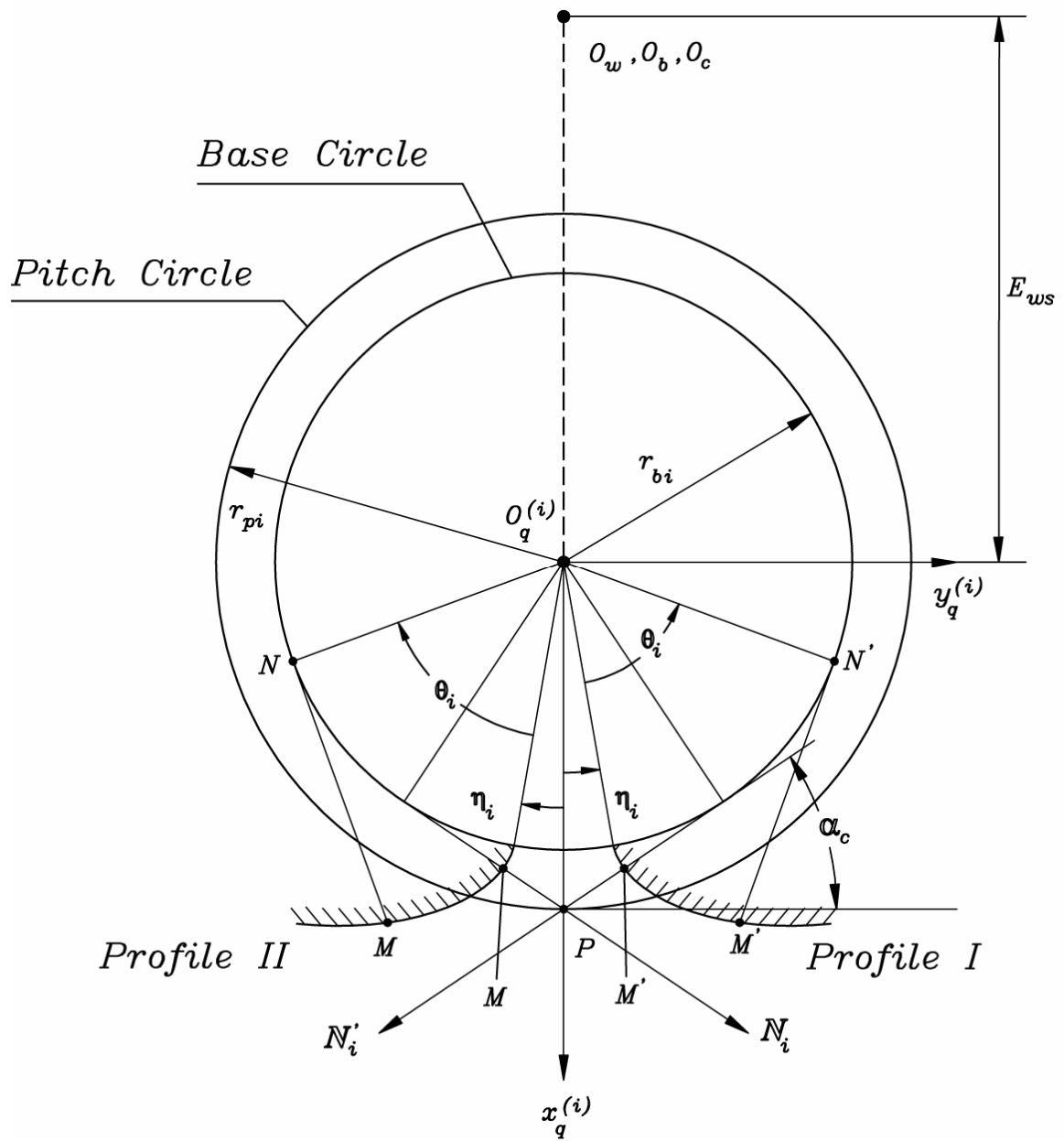


Figure 3.—Shaper profiles and normals to shaper profiles.

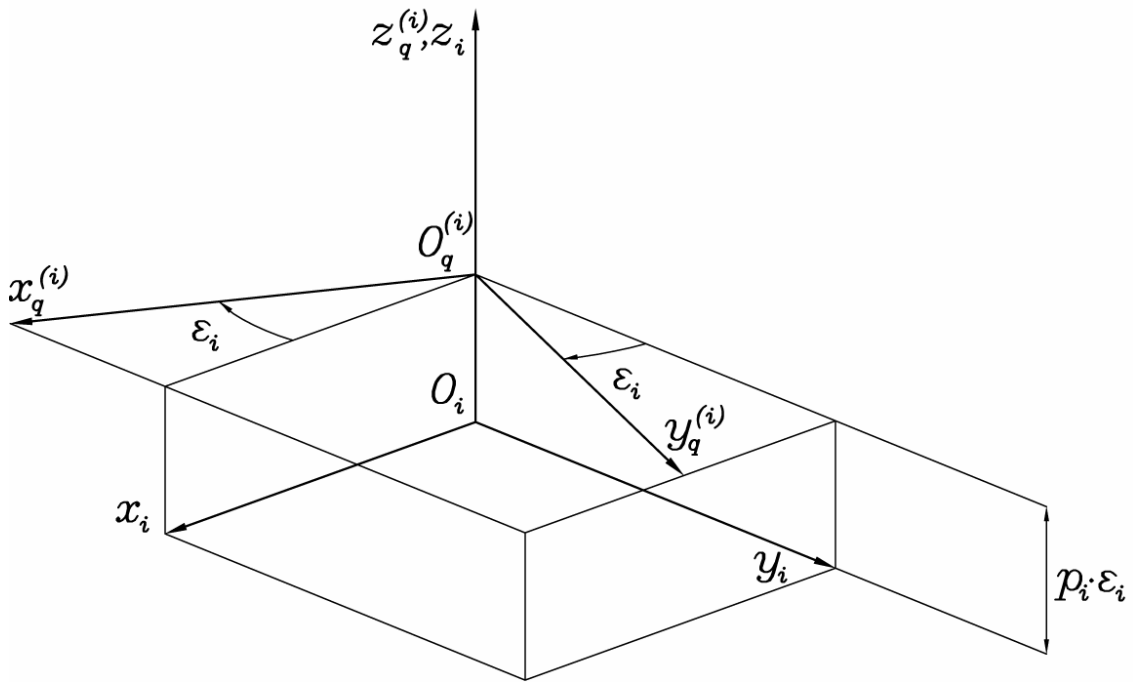
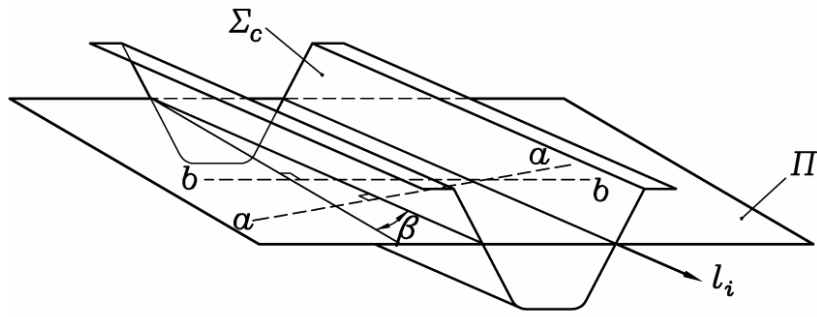
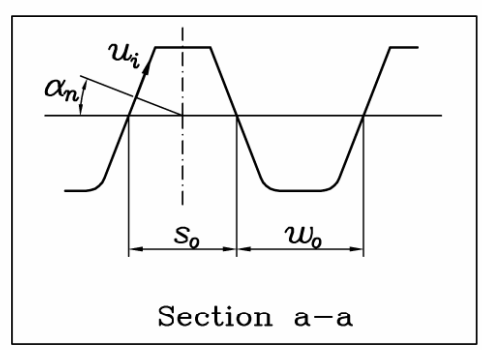


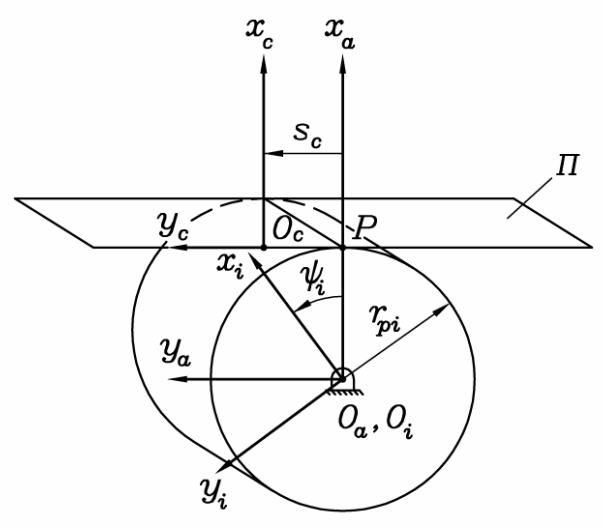
Figure 4.—Illustration of screw motion of coordinate system  $S_q^{(i)}$  with respect to  $S_i$  ( $i = 1, s$ ).



(a)



(b)



(c)

Figure 5.—For derivation of pinion and shaper surfaces  $\Sigma_i$  ( $i = 1,s$ ):  
 (a) skew teeth of the rack-cutter surface  $\Sigma_c$ ; (b) normal section of  $\Sigma_c$ ;  
 (c) coordinate systems used in the meshing between  $\Sigma_c$  and  $\Sigma_i$  ( $i = 1,s$ ).



(a)



(b)

Figure 6.—Solid model of the shaper: (a) whole shaper and (b) detail of the rounded top of the shaper.

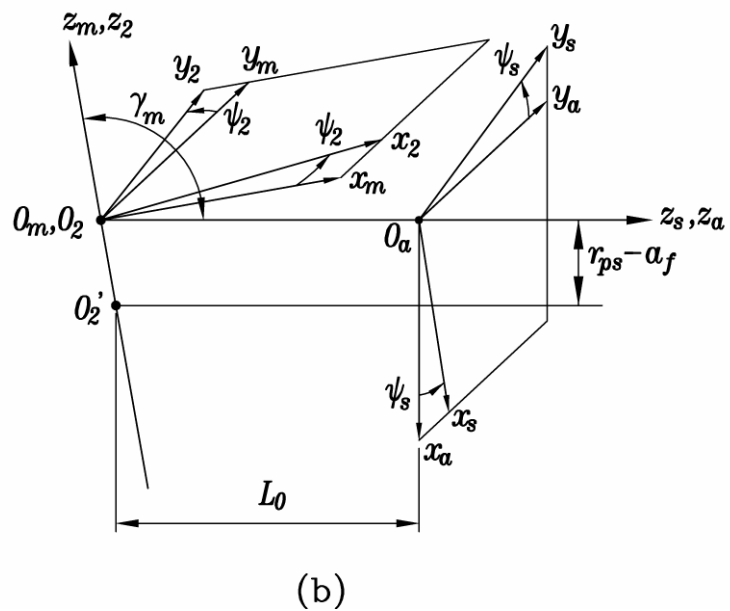
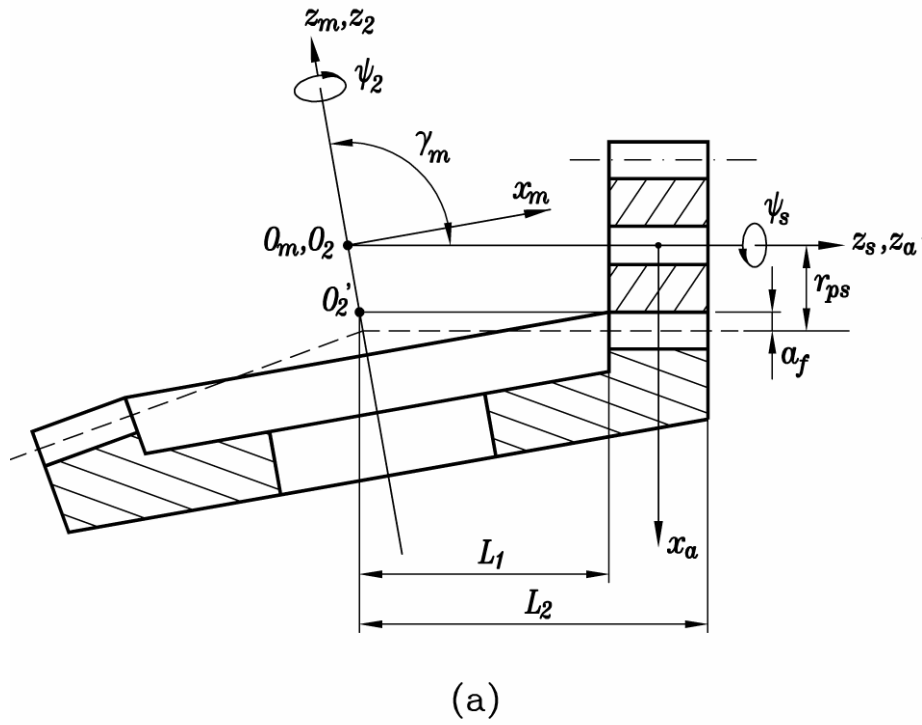


Figure 7.—Coordinate systems applied for generation of face-gear surface  $\Sigma_2$  :  
 (a) illustrates fixed coordinate systems  $S_m$  and  $S_a$  ; (b) illustrates movable  
 coordinate systems  $S_s$  and  $S_2$  .

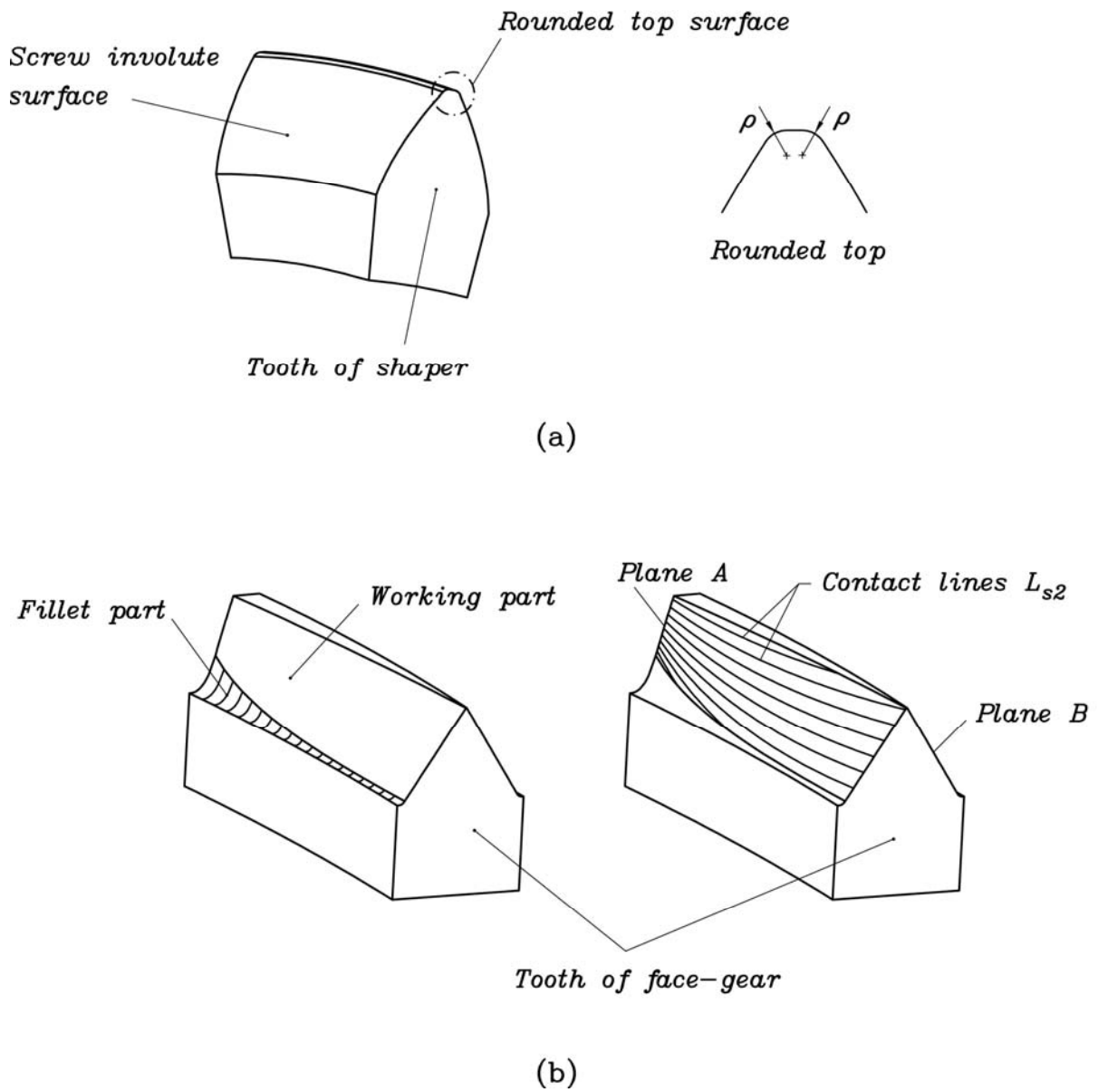


Figure 8.—Structure of shaper and face-gear tooth surface: (a) shows the screw involute surface and the rounded top surface of the shaper, (b) shows the working and fillet parts of the face-gear.

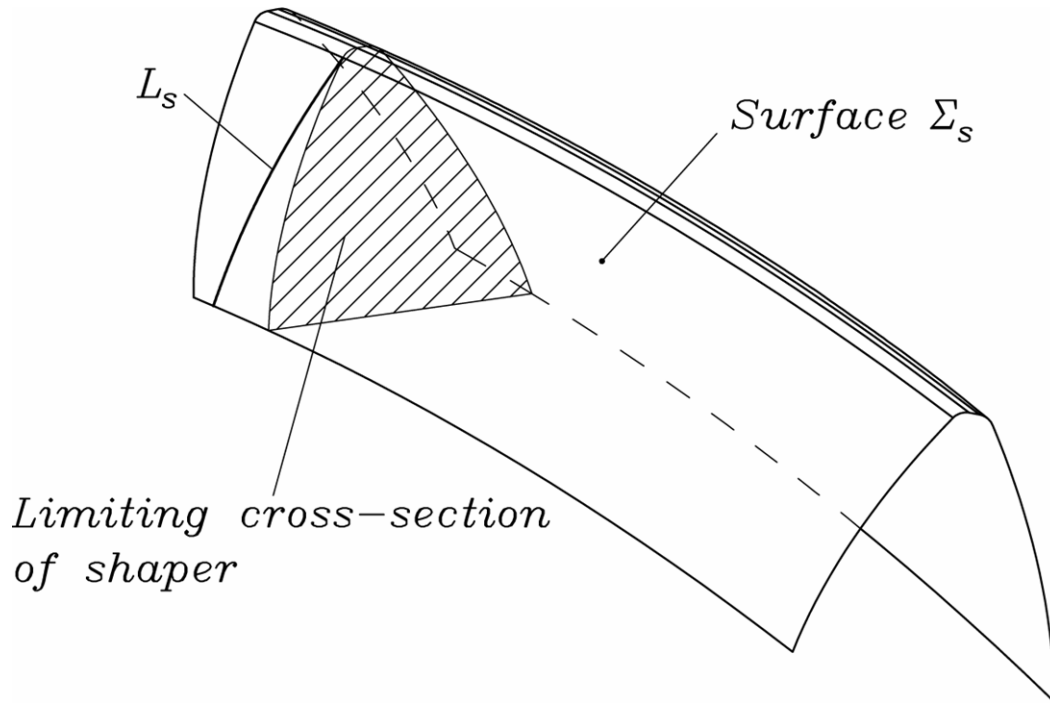


Figure 9.—Illustration of limiting line  $L_s$  on the shaper that generates singular points on  $\Sigma_2$ .

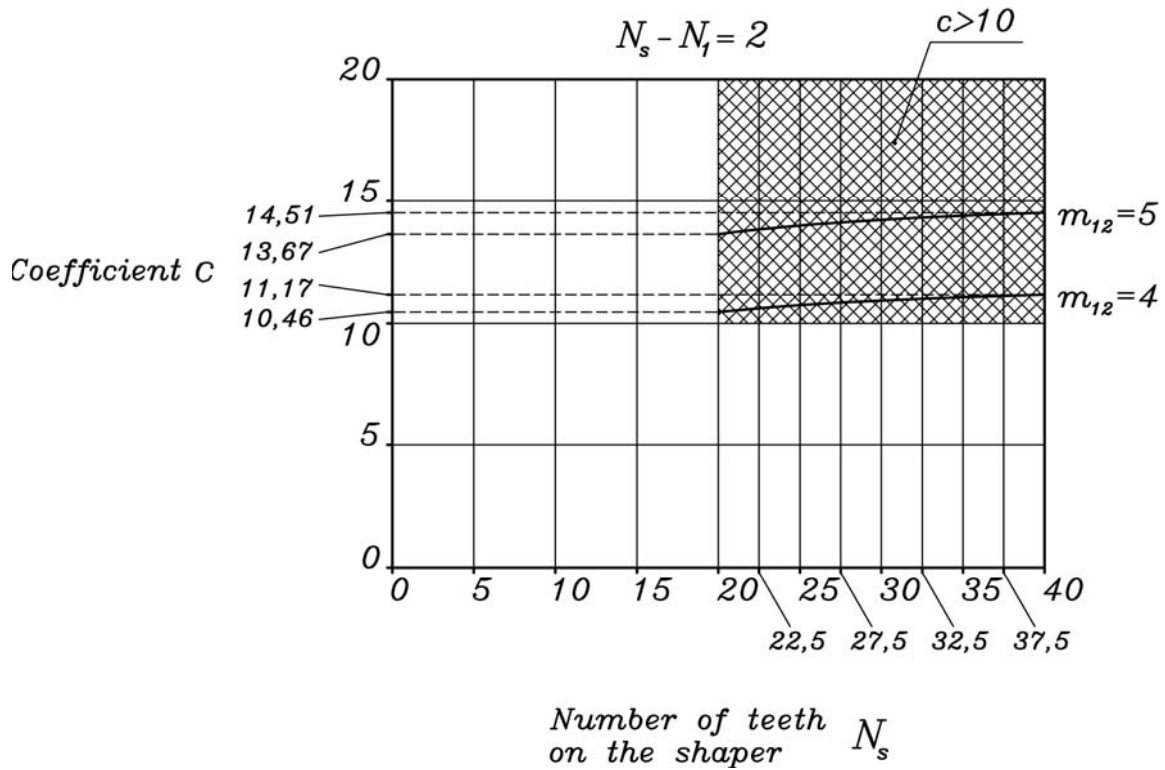


Figure 10.—Graphs of unitless coefficient  $c$  for the case of helix angle  $\beta = 5^\circ$ .

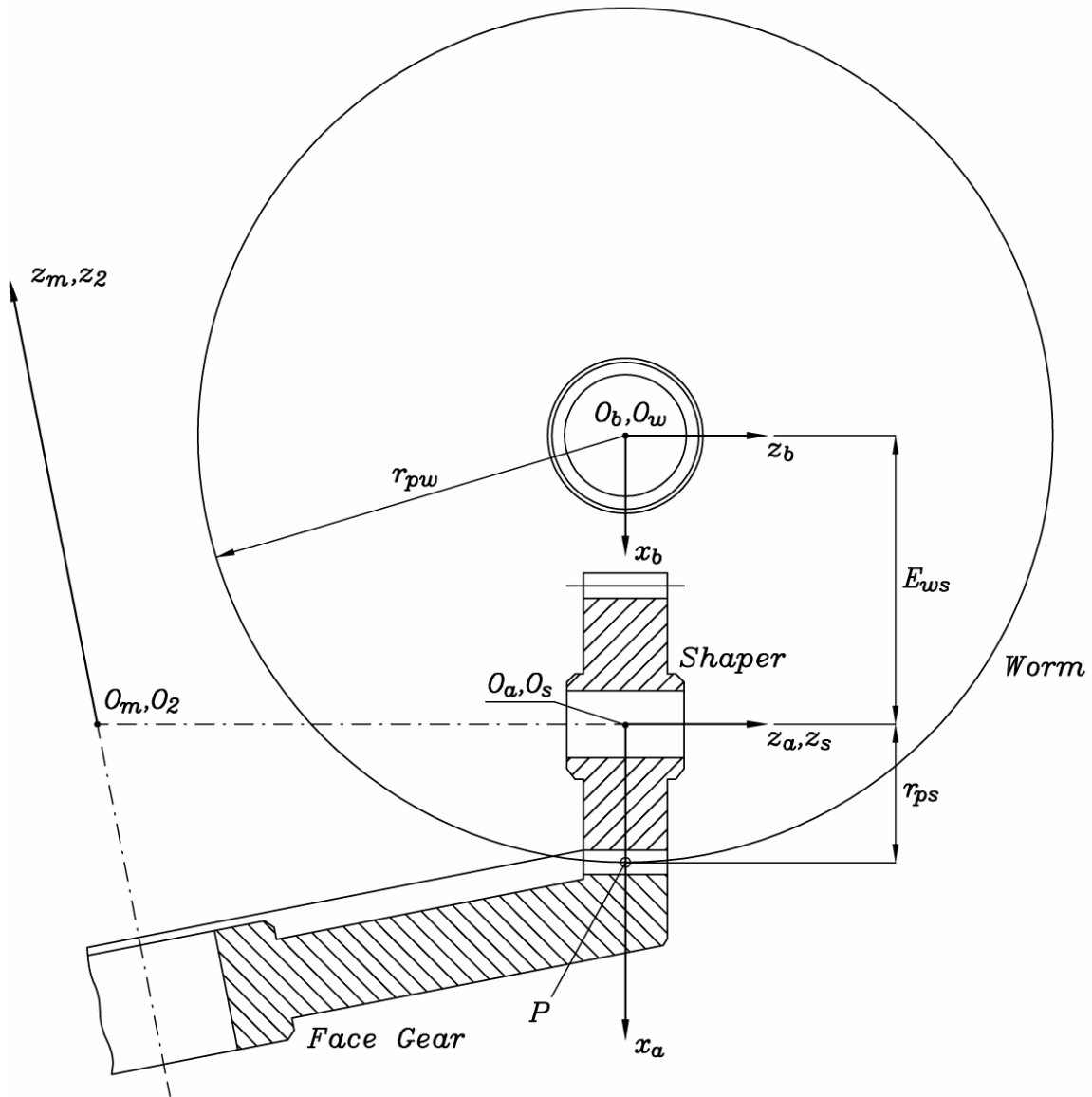


Figure 11.—Schematic illustration of tangency of face gear, shaper, and worm at point P.



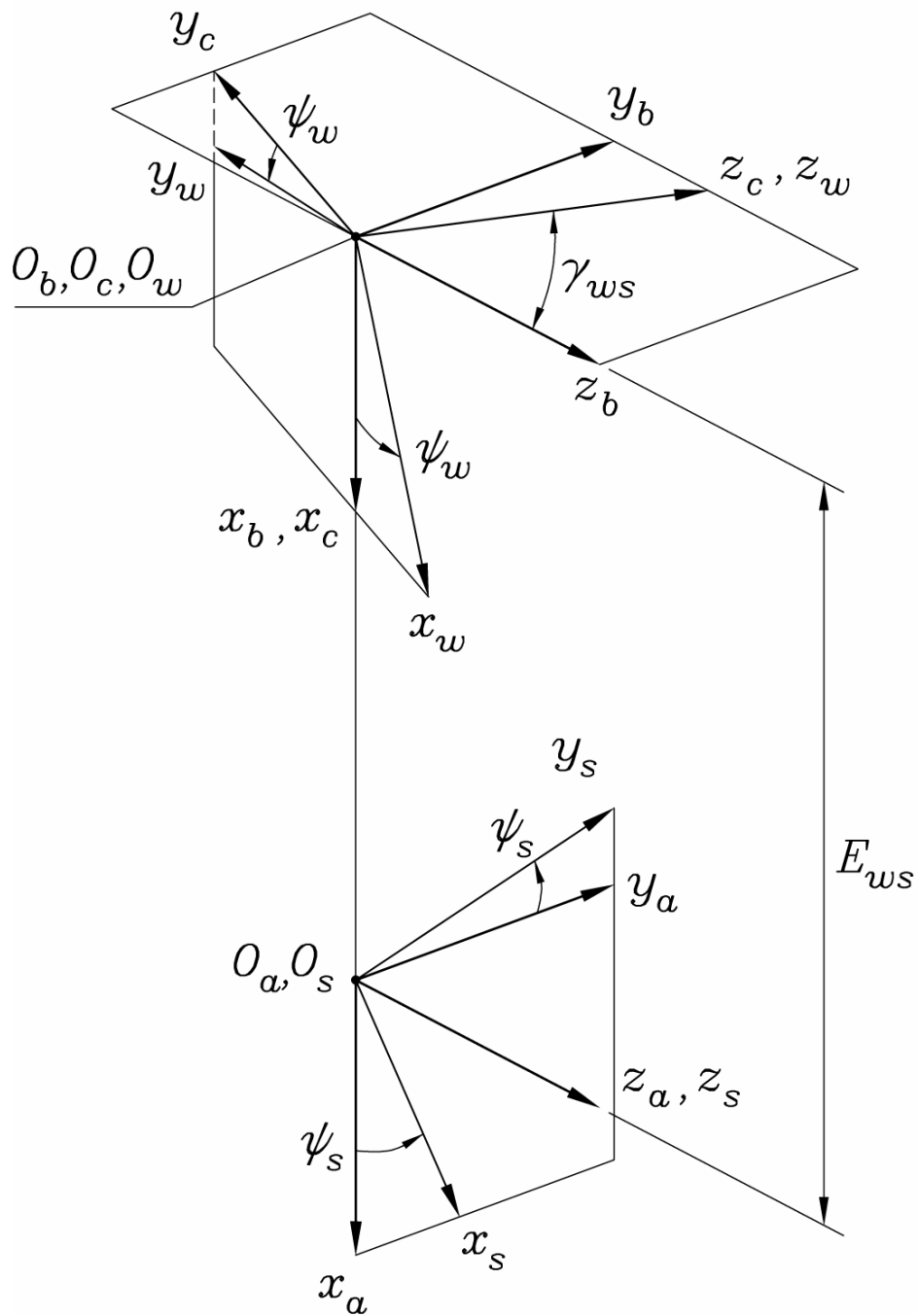
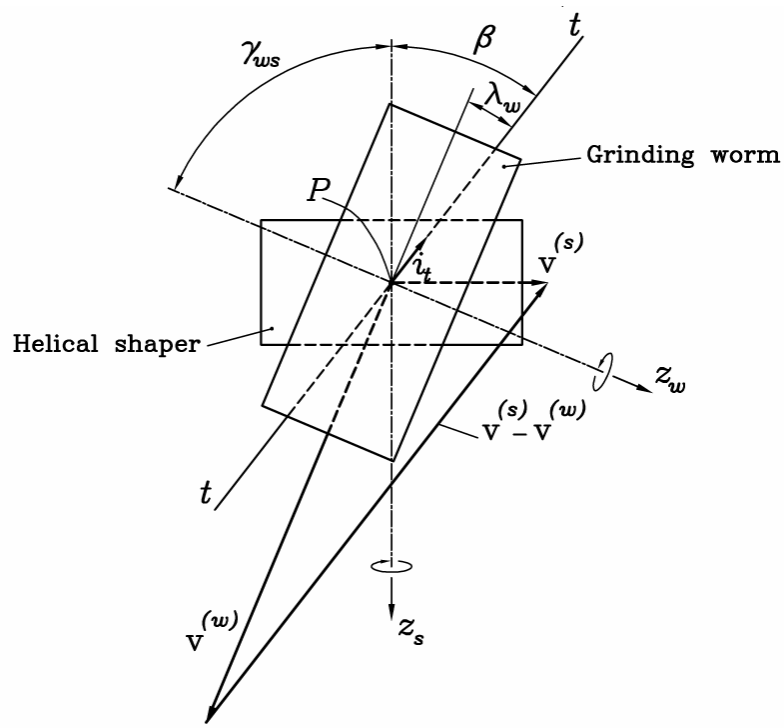
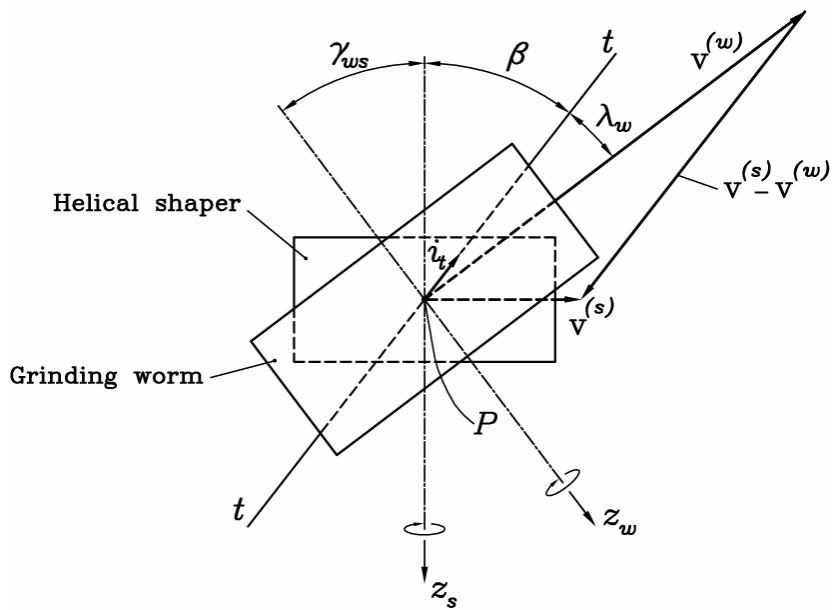


Figure 12.—Coordinate systems used for the derivation of the worm.



(a)



(b)

Figure 13.—For derivation of crossing angle  $\gamma_{ws}$  between the worm and the shaper using: (a) a right-hand worm, (b) a left-hand worm.

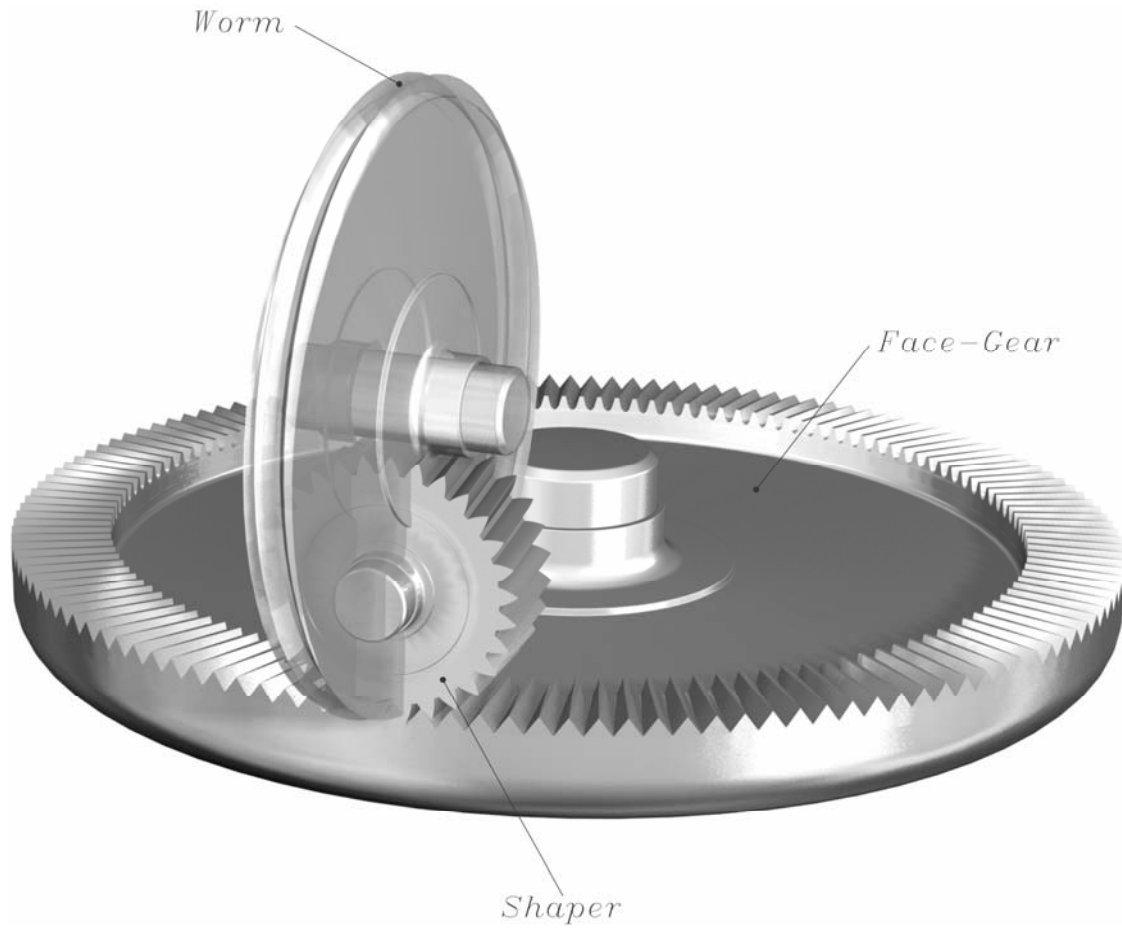
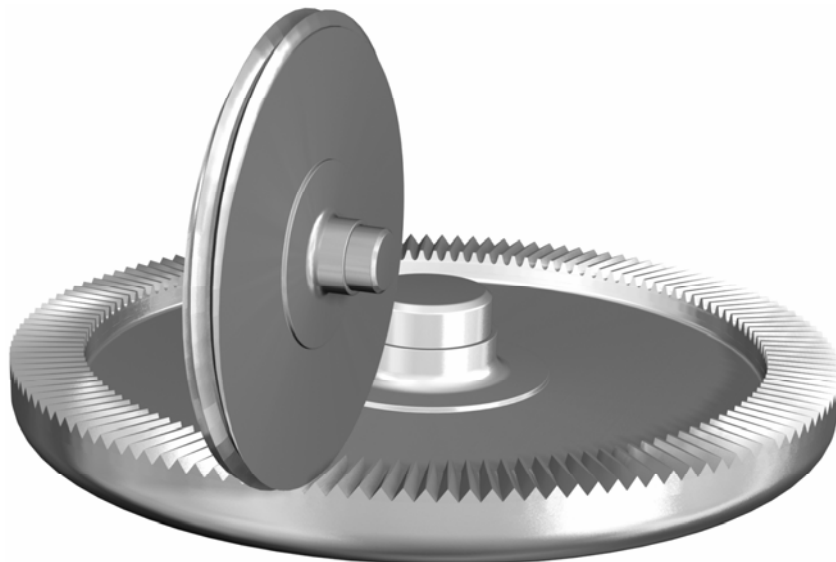


Figure 14.—Illustration of simultaneous meshing of the worm, shaper, and the face-gear wherein the diameter of the worm is larger than the shaper diameter.



(a)



(b)

Figure 15.—Illustration of meshing of: (a) the shaper and the face-gear, and (b) the worm and the face-gear, wherein the worm diameter is chosen larger than the shaper diameter.



Figure 16.—Illustration of simultaneous meshing of the worm, shaper, and the face-gear wherein the worm diameter is less than the shaper diameter.

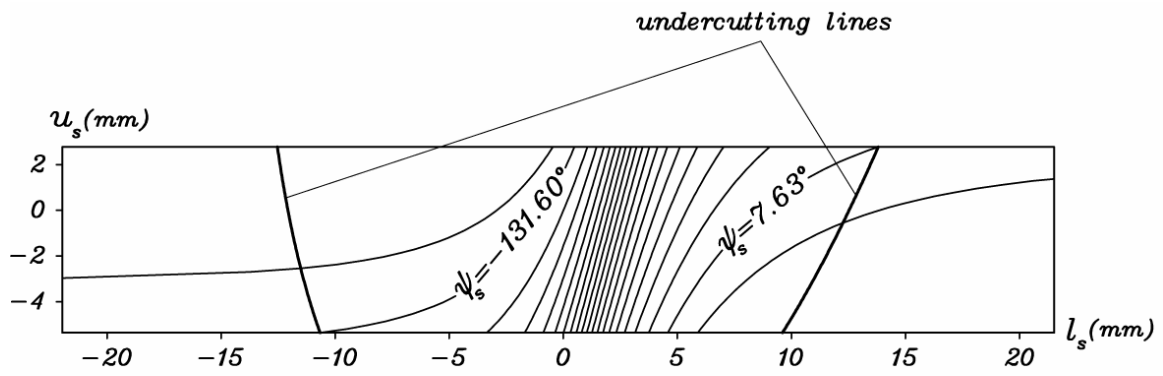


(a)

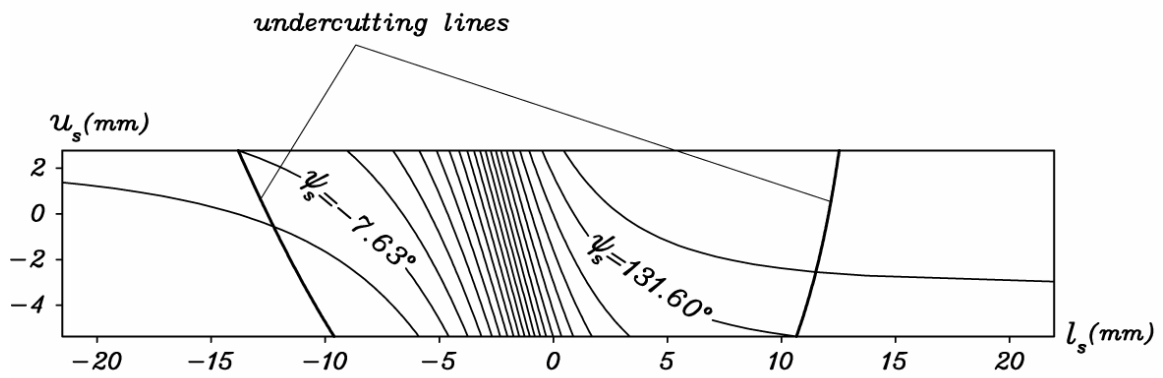


(b)

Figure 17.—Illustration of meshing of: (a) the shaper and the face-gear, and (b) the worm and the face-gear, wherein the worm diameter is chosen lesser than the shaper diameter.

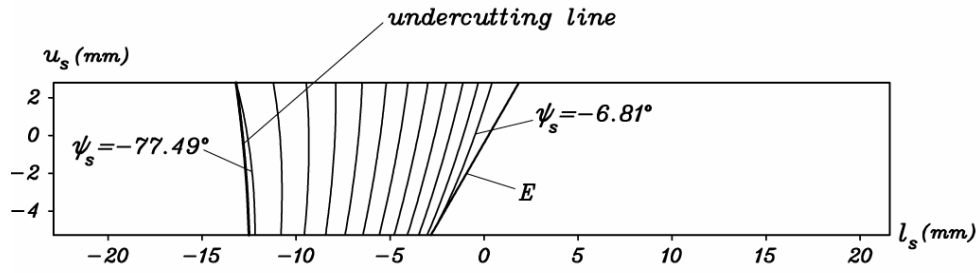


(a)

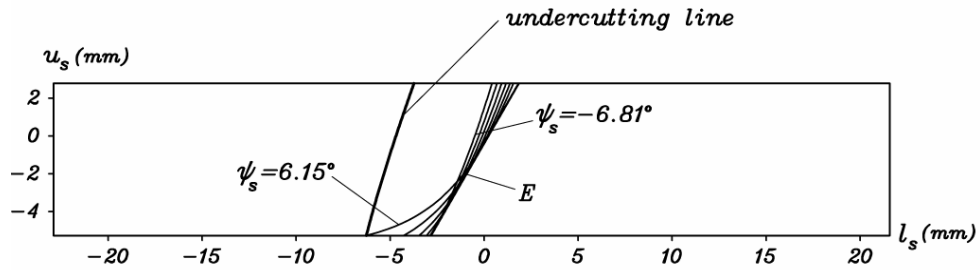


(b)

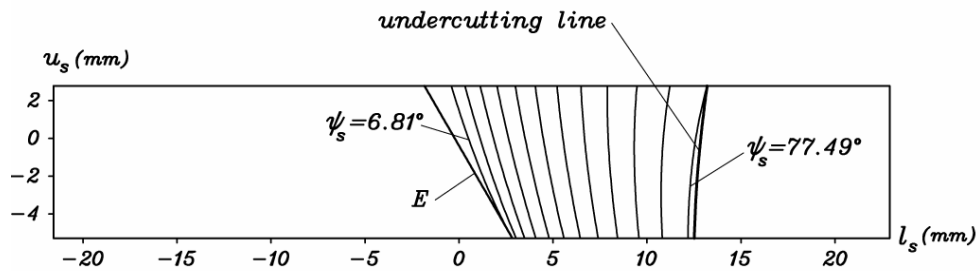
Figure 18.—Lines of contact and undercutting lines for a shaper of helix angle of  $5^\circ$  :  
 (a) for the drive side, and (b) for the coast side.



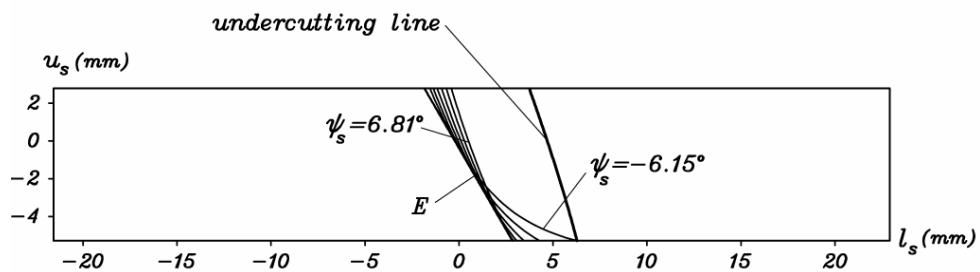
(a)



(b)



(c)



(d)

Figure 19.—Lines of contact and undercutting lines, and envelope E to the family of contact lines: (a) and (b) contact lines on the drive side in two regions where each region is formed between the undercutting line and envelope E to the family of contact lines; (c) and (d) contact lines on the coast side for two similar regions.



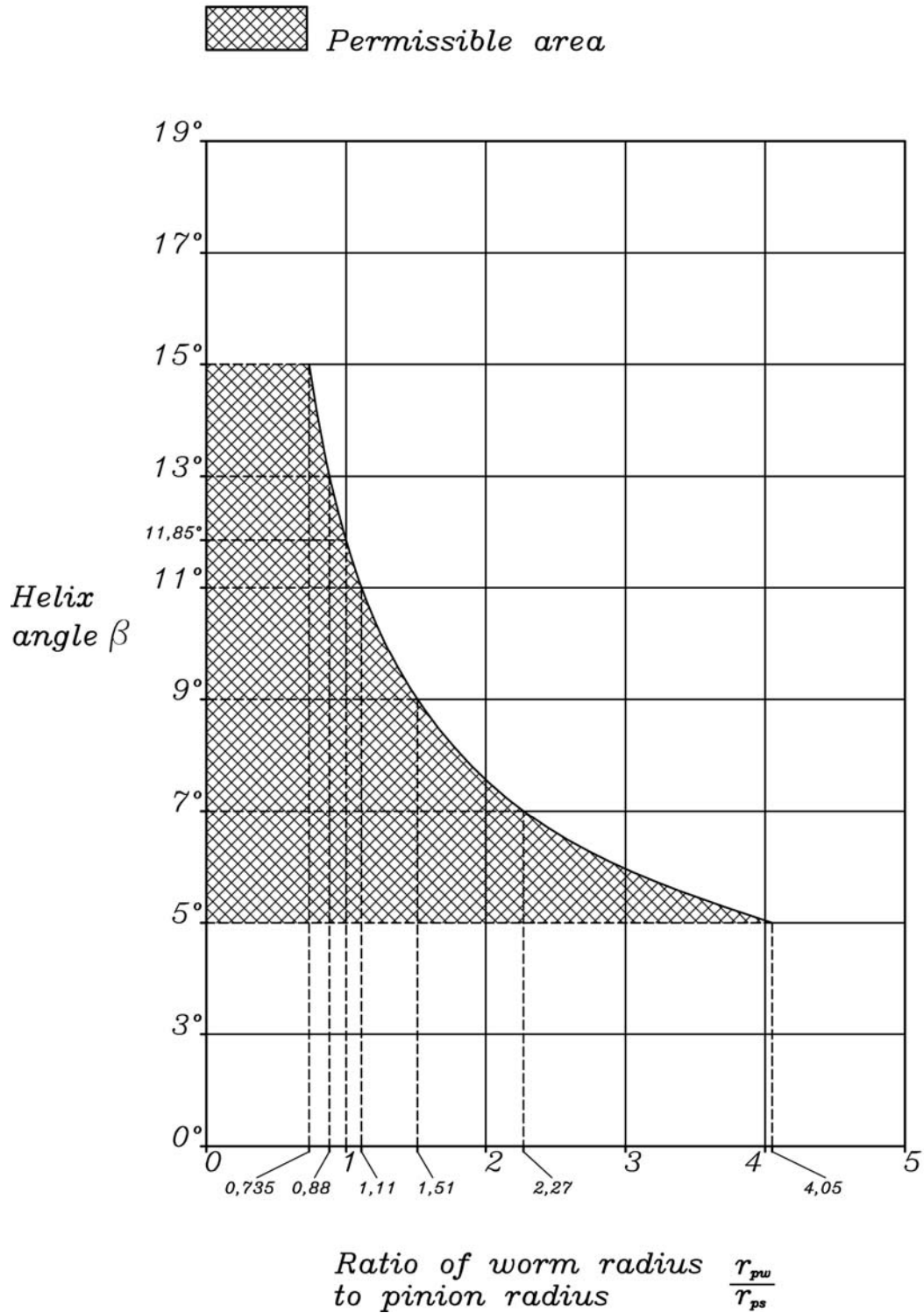
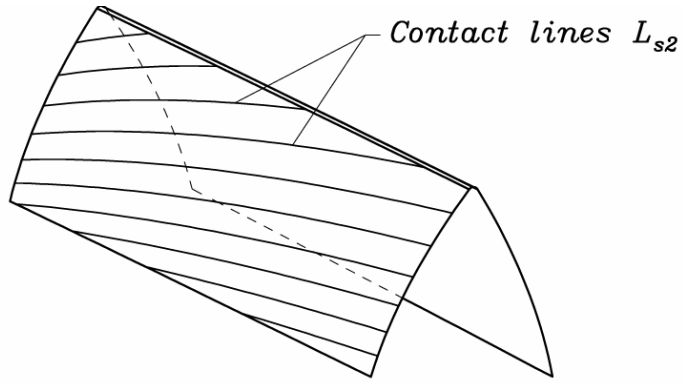
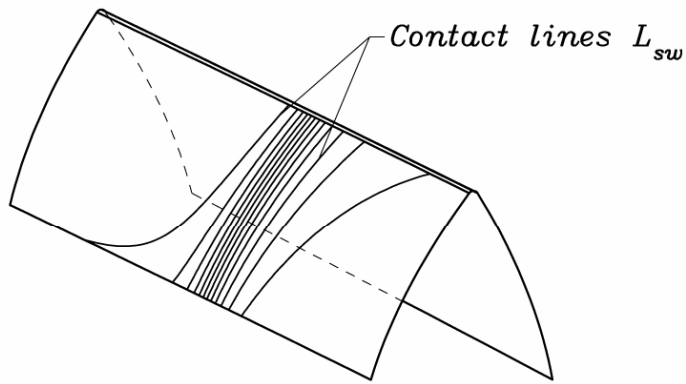


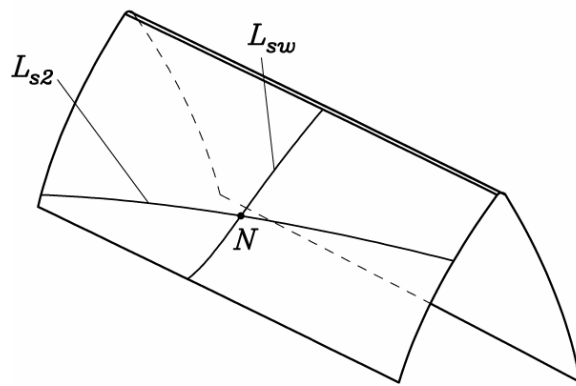
Figure 20.—Illustration of relation of the helix angle of the shaper and the ratio of radii of the pitch cylinders of the worm and the shaper based on data in table 2.



(a)



(b)



(c)

Figure 21.—Contact lines on shaper surface  $\Sigma_s$  : (a) contact lines  $L_{s2}$  between  $\Sigma_s$  and  $\Sigma_2$ , (b) contact lines  $L_{sw}$  between  $\Sigma_s$  and  $\Sigma_w$ , (c) contact lines  $L_{s2}$  and  $L_{sw}$  for a chosen value of the parameter of motion.

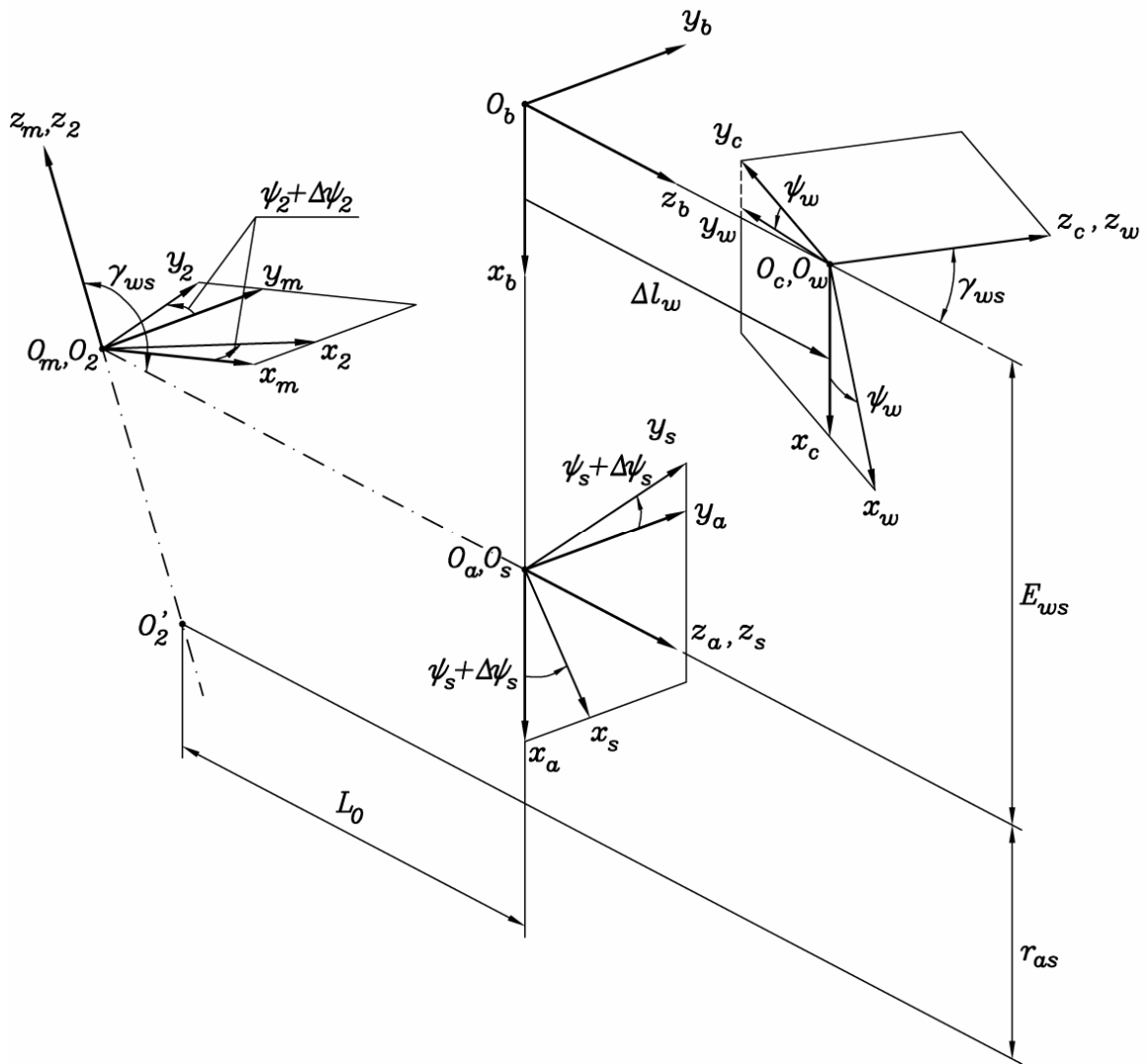


Figure 22.—Coordinate systems applied in the generation of a helical face gear by a worm.

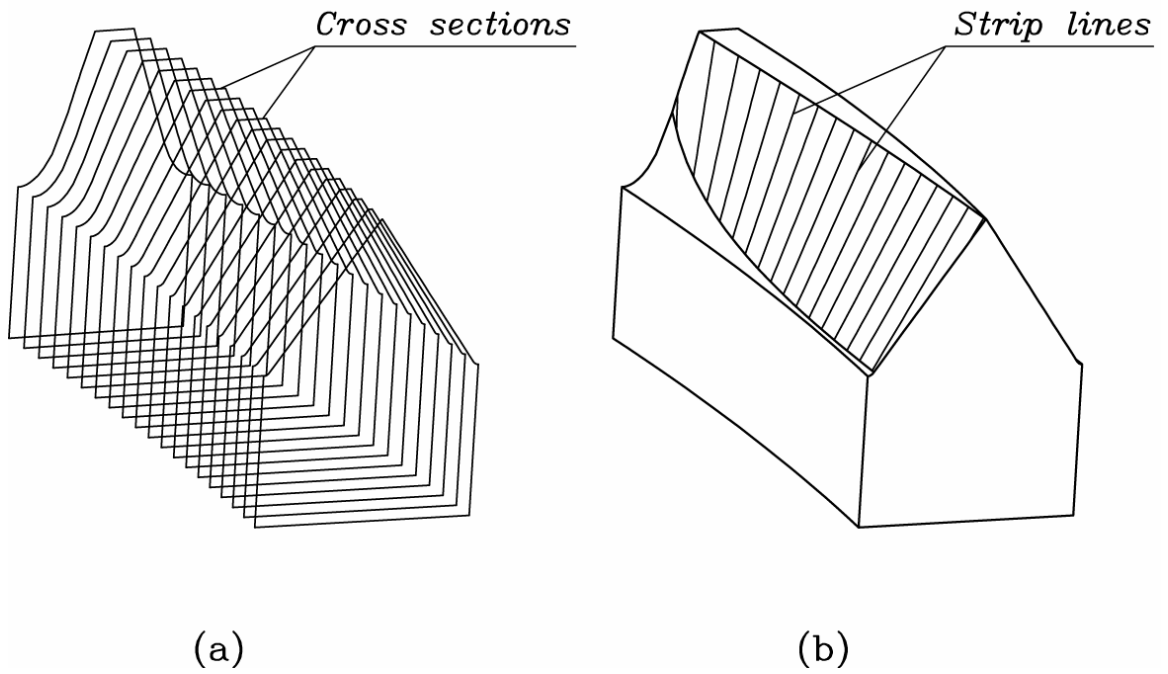


Figure 23.—Illustration of face-gear surface  $\Sigma_2$ : (a) cross sections of  $\Sigma_2$ ; (b) strip lines on  $\Sigma_2$ .

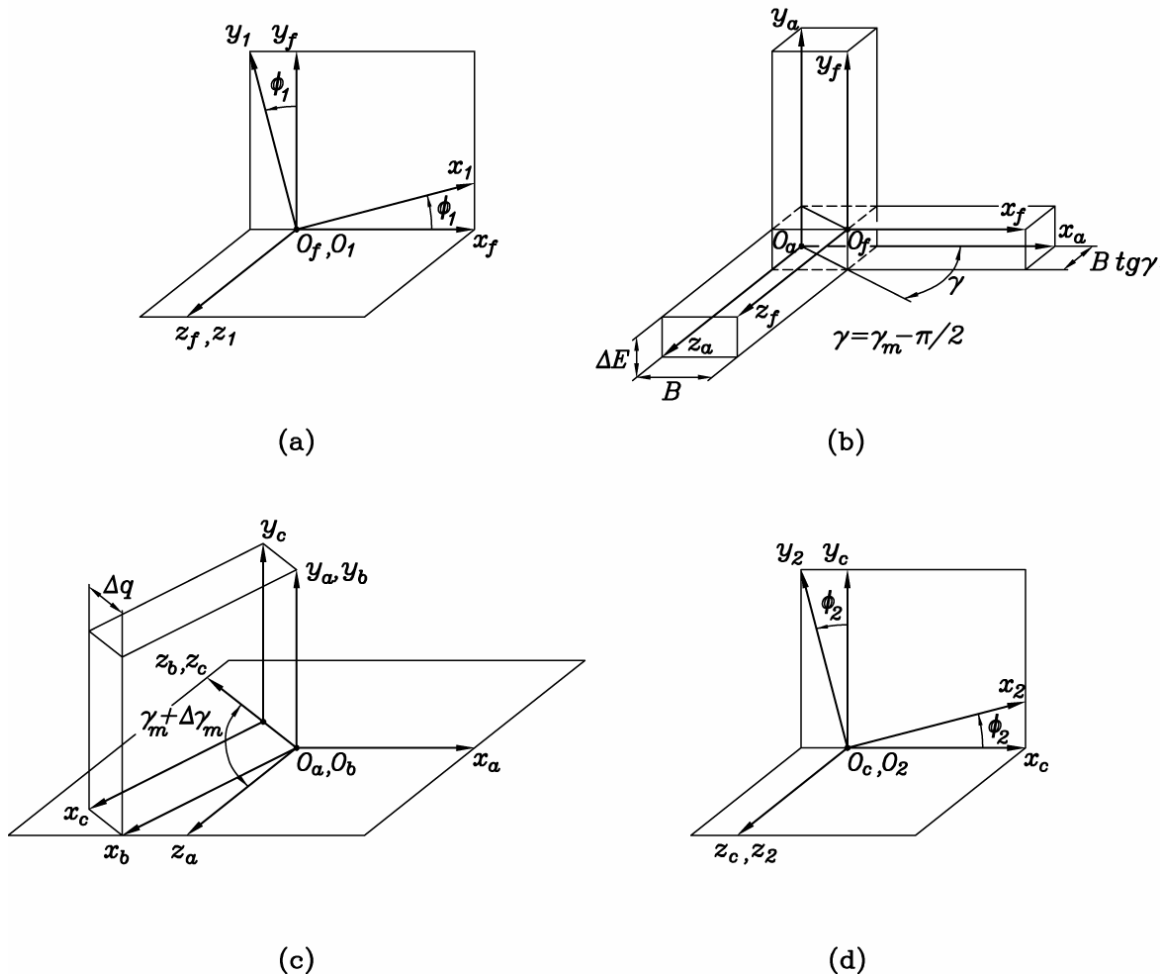


Figure 24.—Coordinate systems applied for simulation of meshing: (a) coordinate systems  $S_1$  and  $S_f$ ; (b) coordinate systems  $S_f$  and  $S_a$ ; (c) coordinate systems  $S_a$ ,  $S_b$ , and  $S_c$ ; (d) coordinate systems  $S_c$  and  $S_2$ .

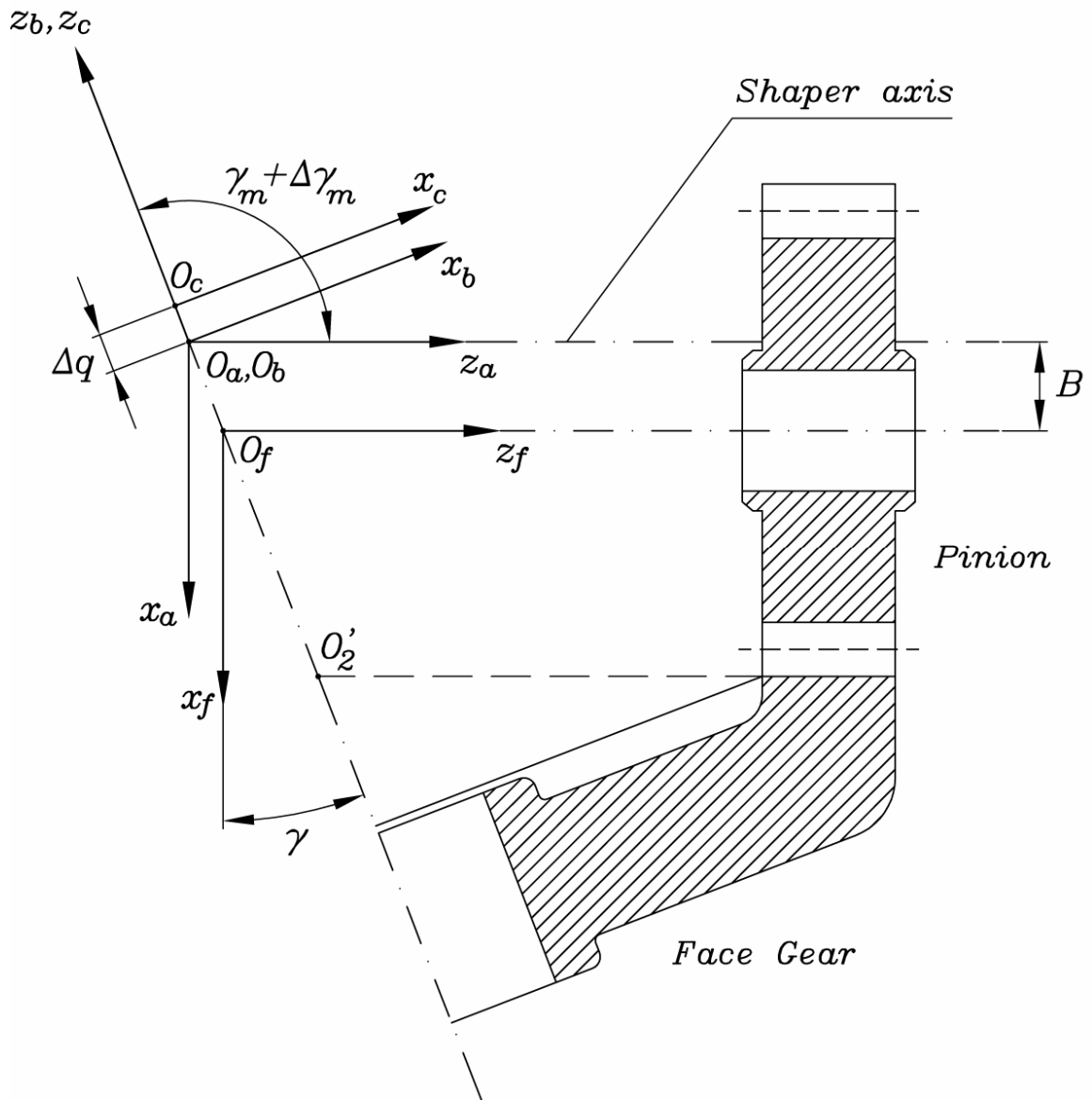
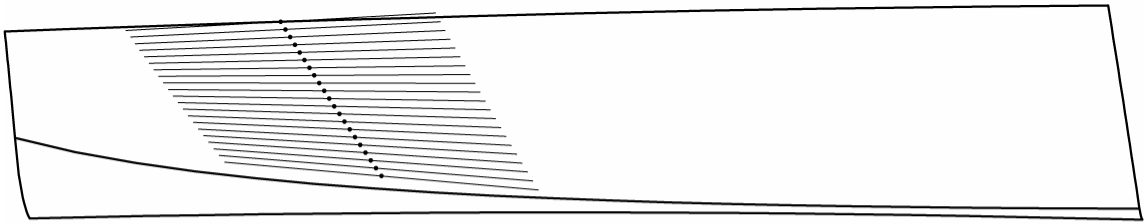
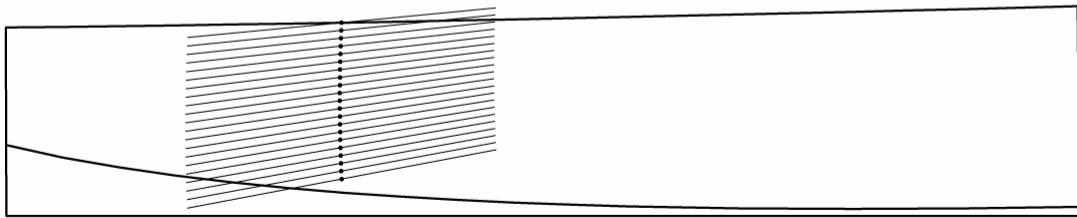


Figure 25.—Coordinate systems  $S_f$ ,  $S_a$ ,  $S_b$ , and  $S_c$  applied for simulation of meshing between the pinion and the face gear.

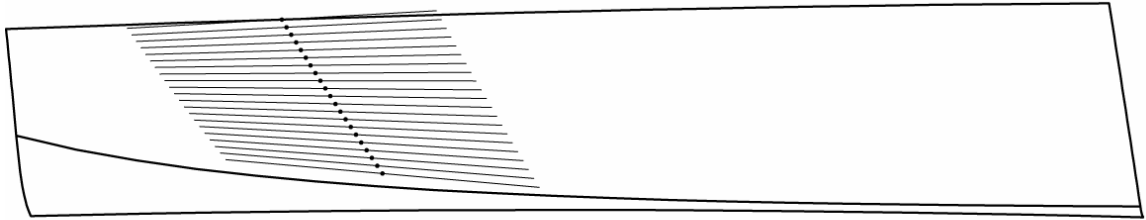


(a)

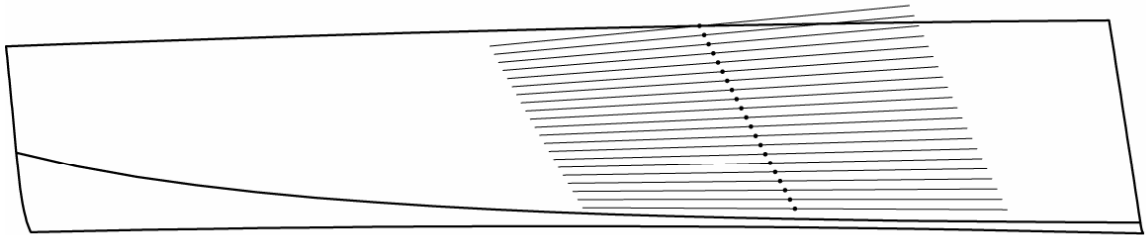


(b)

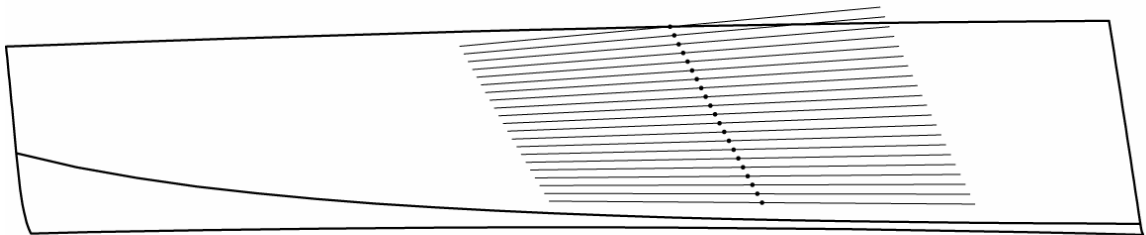
Figure 26.—Illustration of path of contact of an aligned gear drive: (a) for a gear drive with a helical pinion, and (b) for a gear drive with a spur pinion.



(a)



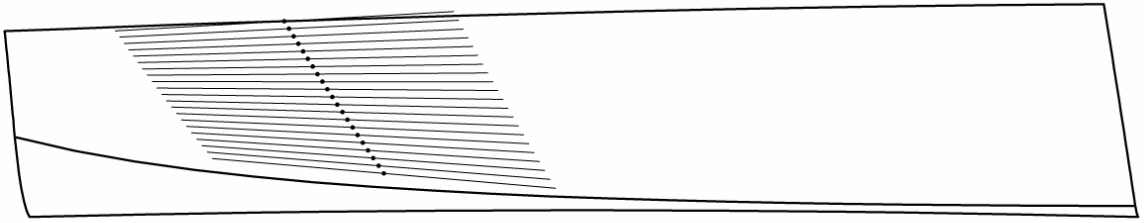
(b)



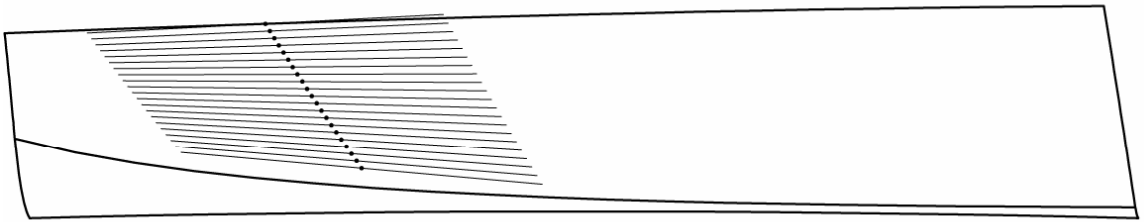
(c)

Figure 27.—Path of contact and bearing contact on face-gear surface with a helical pinion:  
 (a) no errors of alignment; (b)  $\Delta\gamma_m = 3$  arcmin; (c)  $\Delta E = -1$  mm.

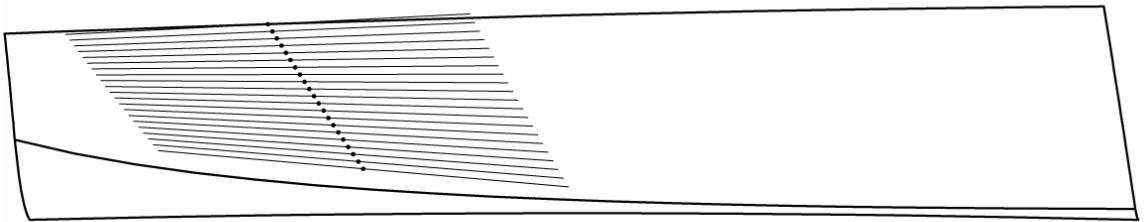




(a)



(b)



(c)

Figure 28.—Illustration of compensation of shift of bearing contact by application of correction  $\Delta q$ : (a)  $\Delta\gamma_m = 3$  arcmin,  $\Delta q = -550$   $\mu\text{m}$ ; (b)  $\Delta E = -1000$   $\mu\text{m}$ ,  $\Delta q = -500$   $\mu\text{m}$ ; (c)  $\Delta\gamma_m = 3$  arcmin,  $\Delta E = -1000$   $\mu\text{m}$ ,  $\Delta q = -1050$   $\mu\text{m}$ .

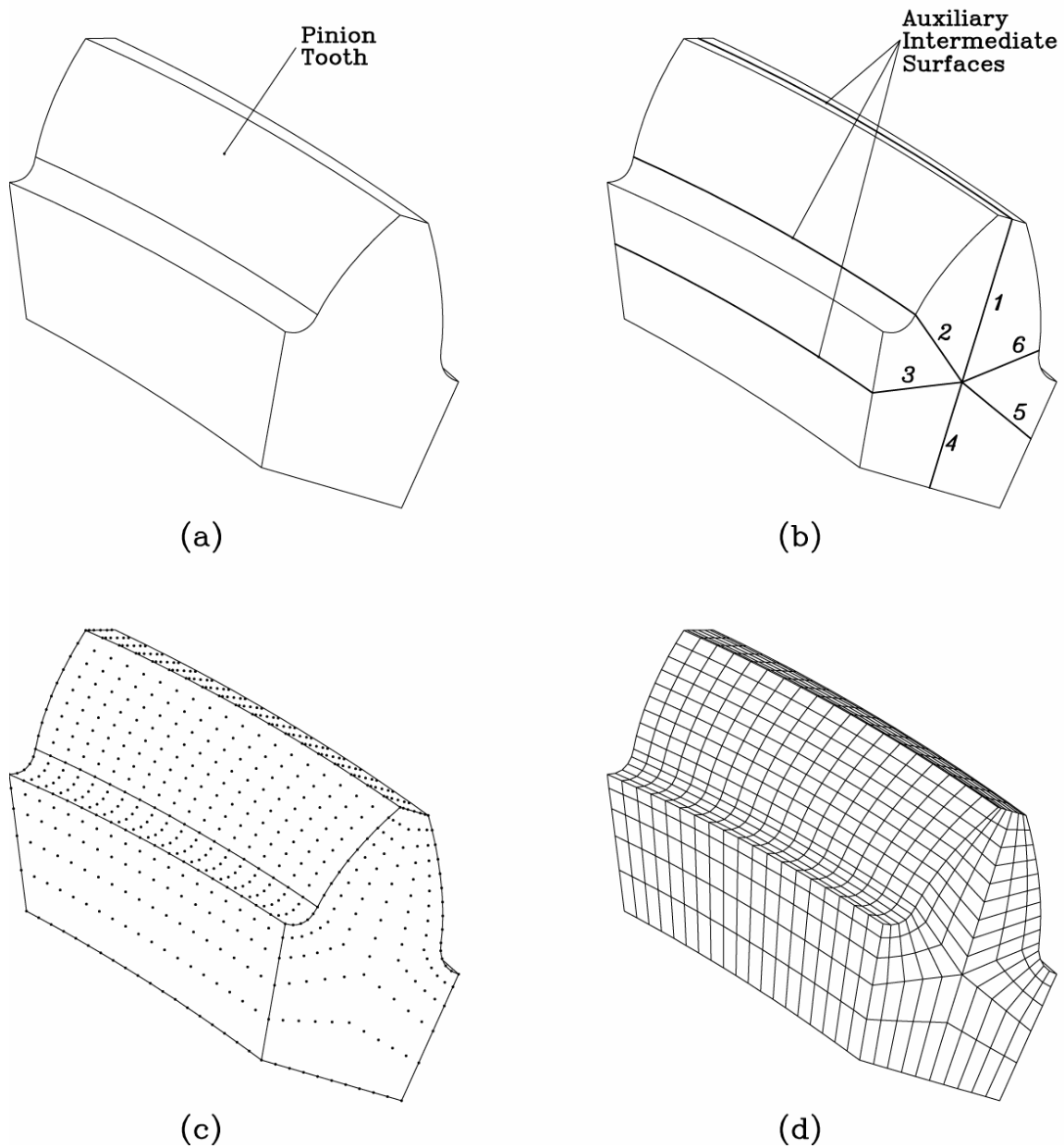


Figure 29.—Illustrations of: (a) the volume of designed body, (b) auxiliary intermediate surfaces, (c) determination of nodes for the whole volume, and (d) discretization of the volume by finite elements.

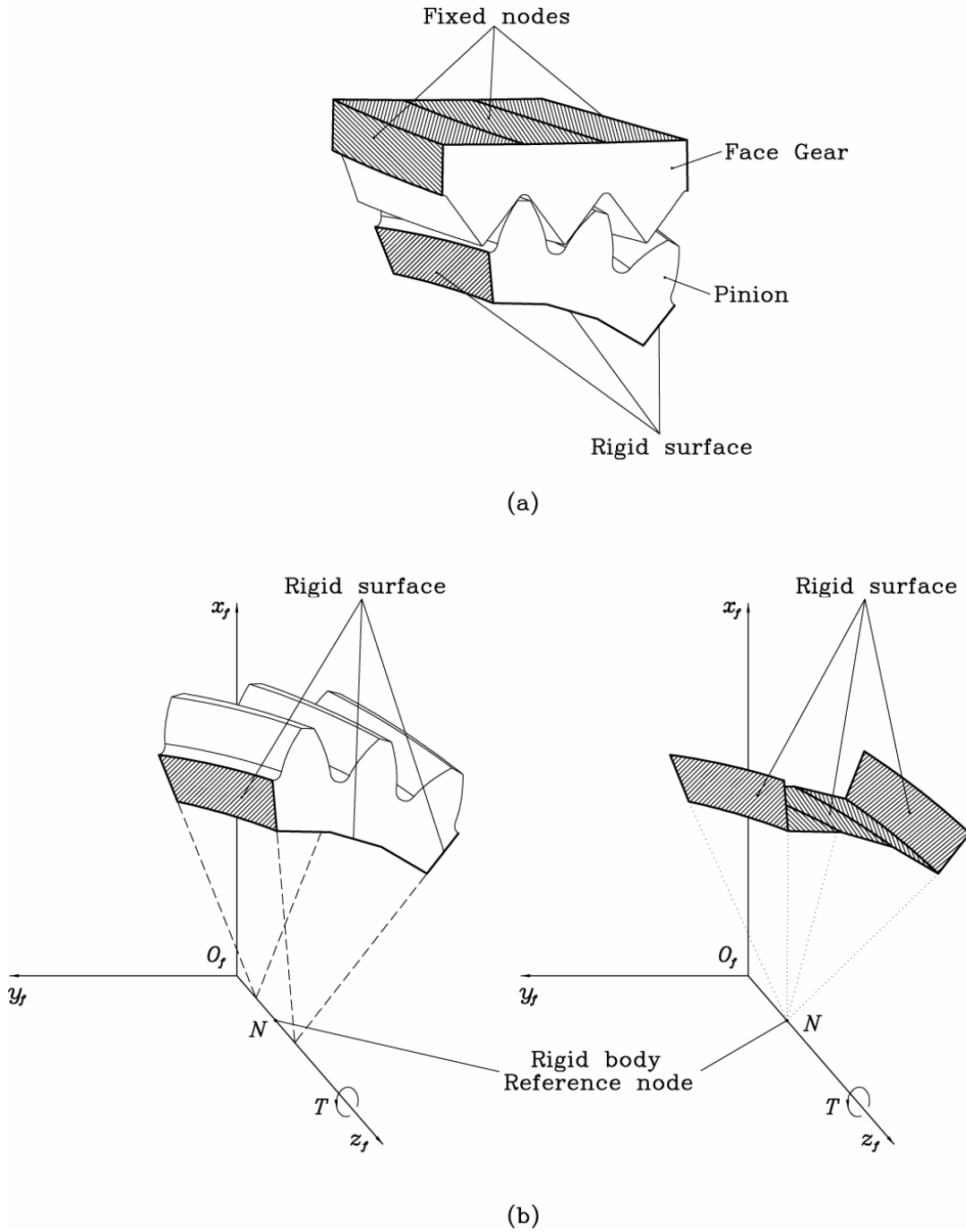


Figure 30.—Schematic illustration of: (a) boundary conditions for the pinion and the face gear, and (b) rigid surfaces applied for boundary conditions of the pinion.

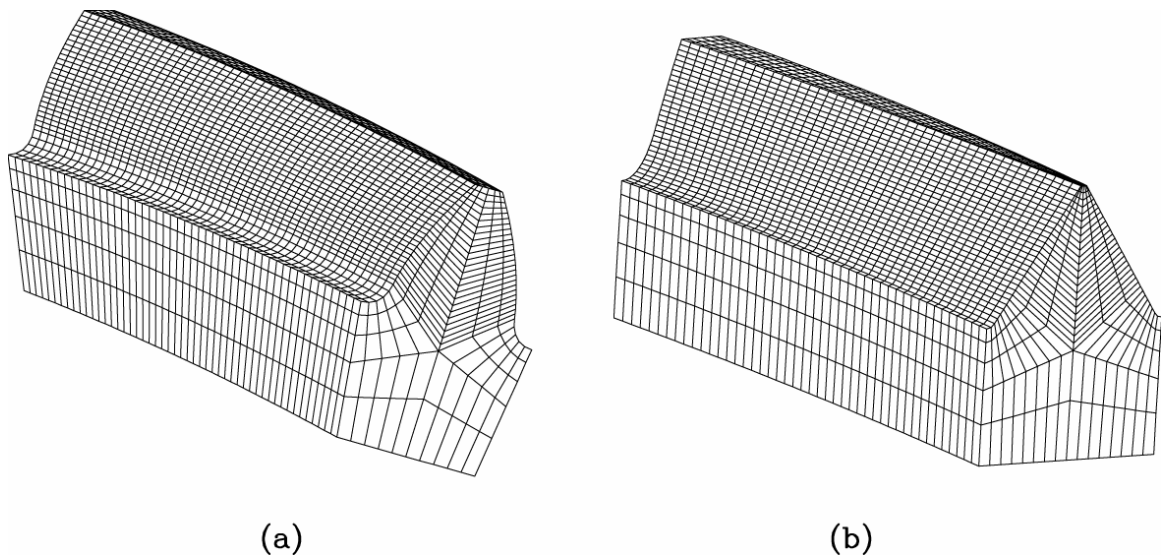


Figure 31.—Finite element models of (a) one-tooth of the pinion and (b) one-tooth of the face gear.

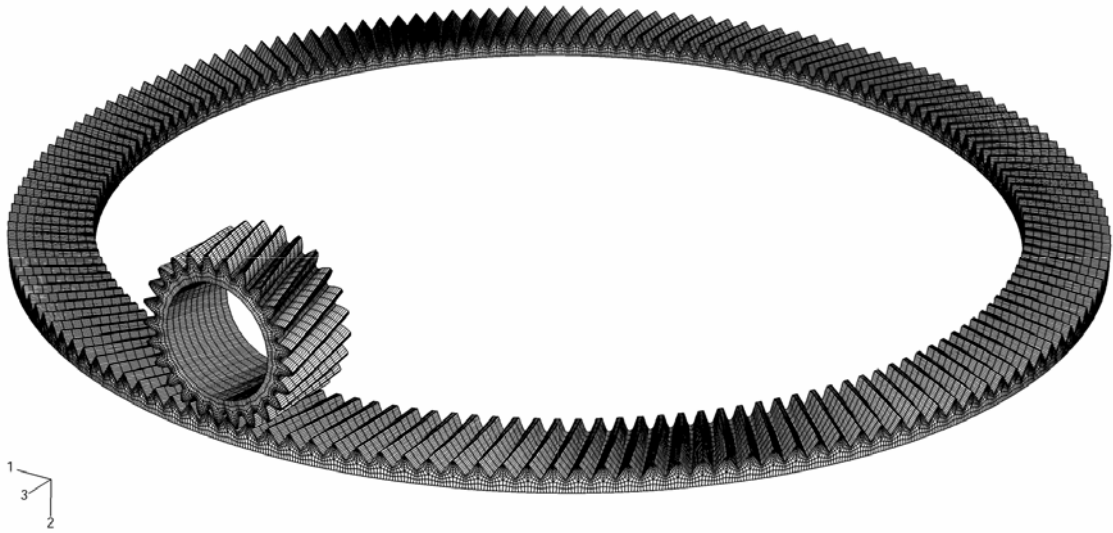


Figure 32.—Whole gear drive finite element model.

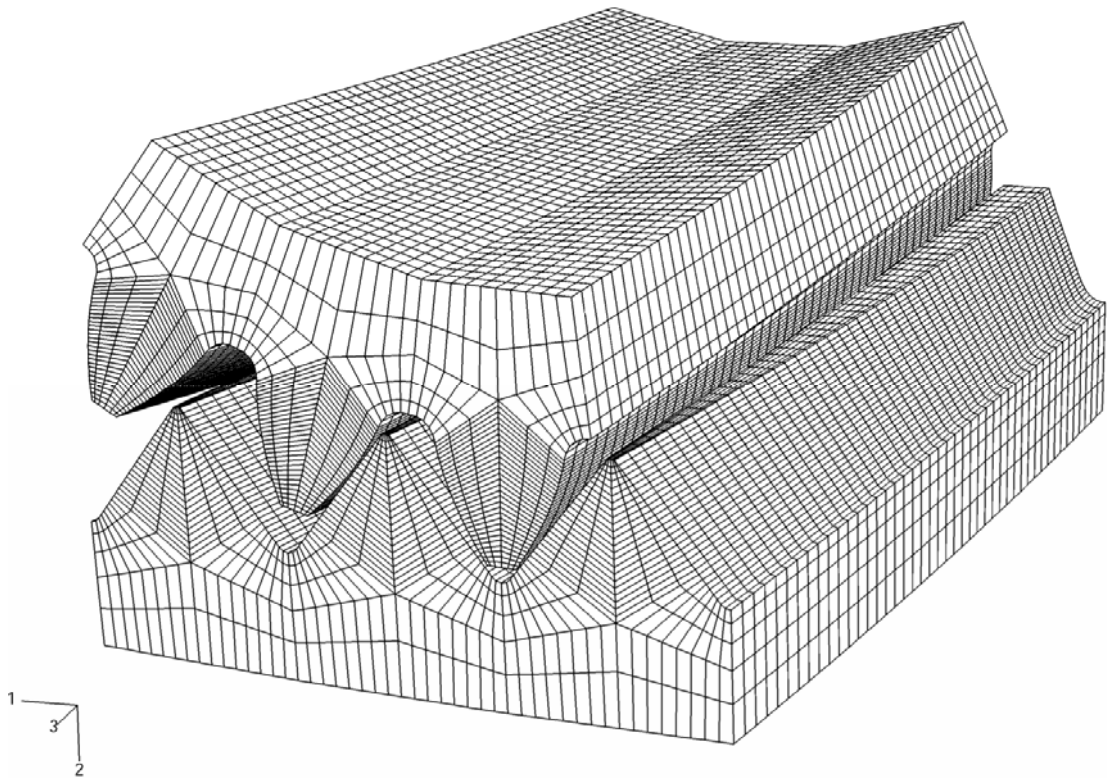


Figure 33.—Finite element model of three pairs of teeth.

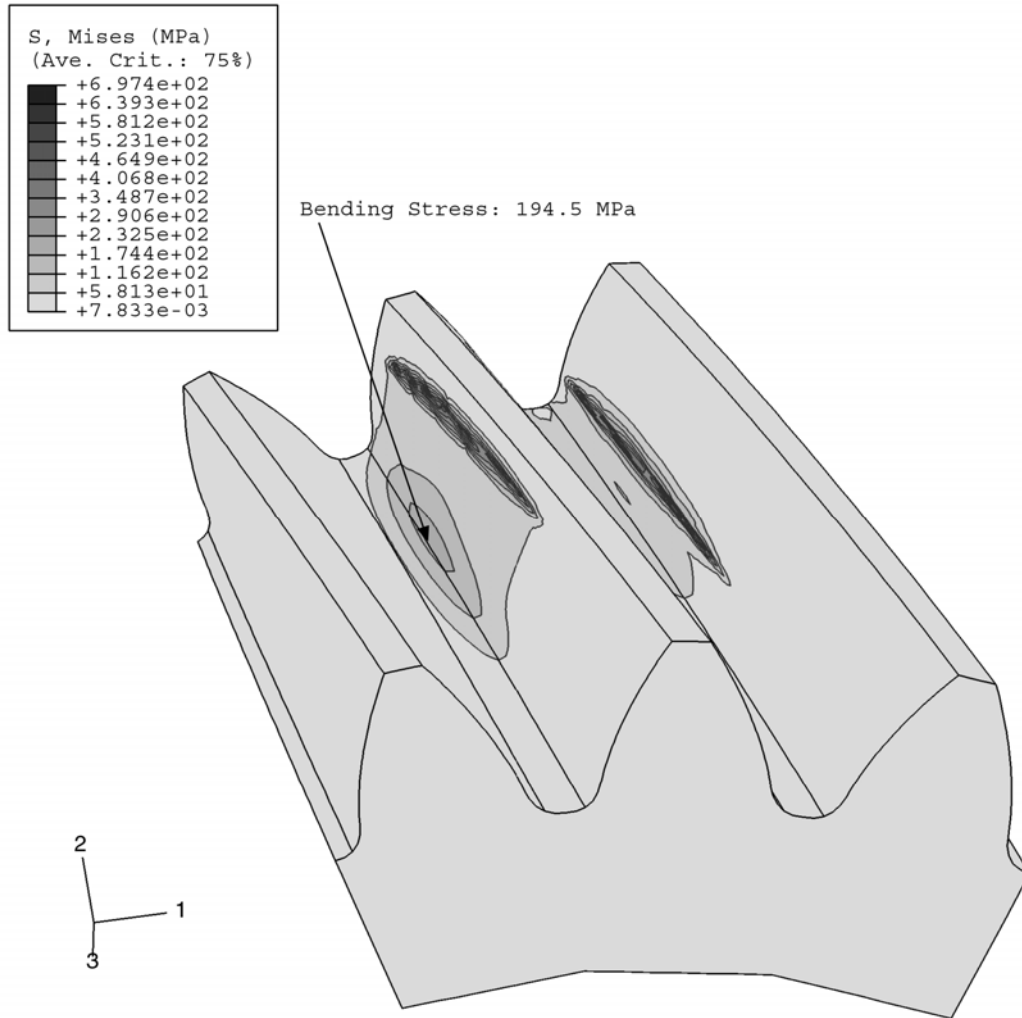


Figure 34.—Contact and bending stresses at a contact point of the helical involute pinion of a face-gear drive.

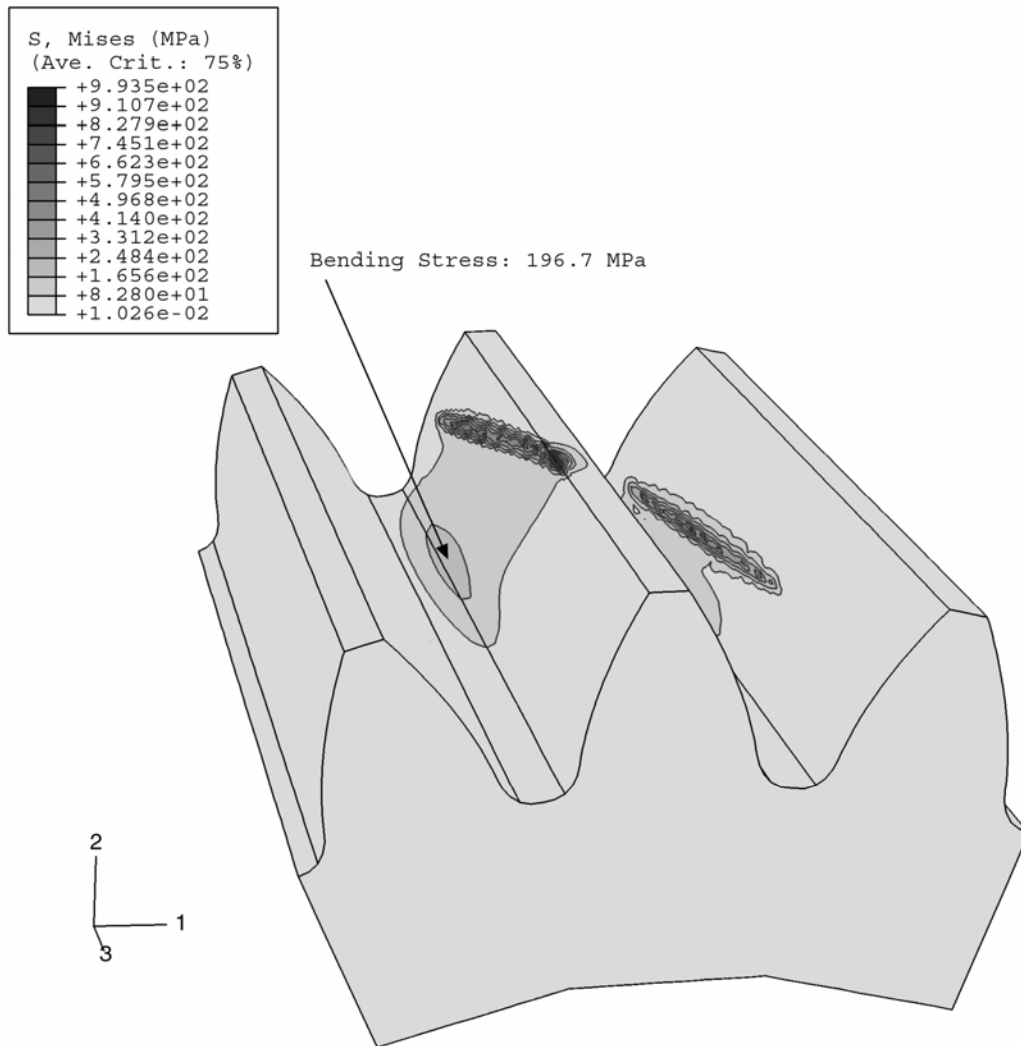


Figure 35.—Contact and bending stresses at a contact point of the spur involute pinion of a face-gear drive.

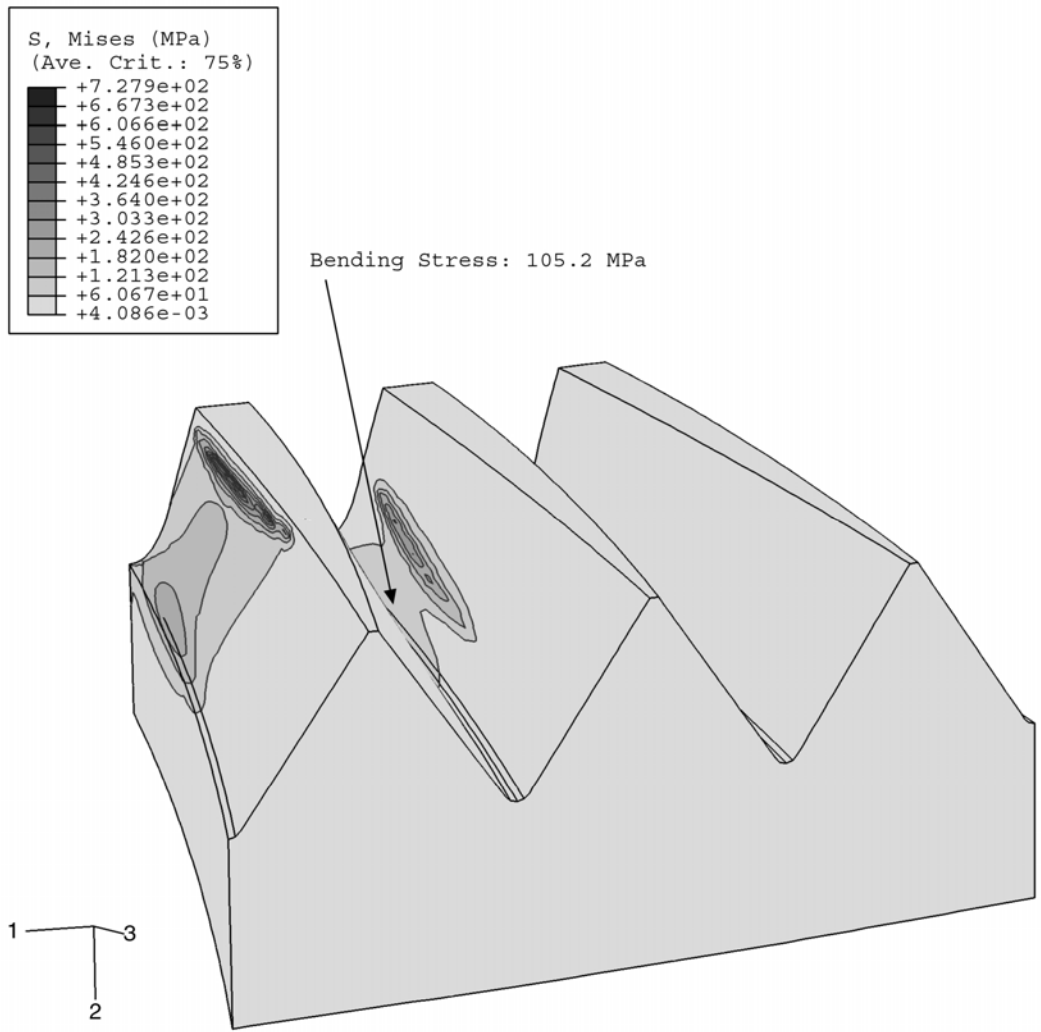


Figure 36.—Contact and bending stresses at a contact point of the face gear of a face-gear drive with helical involute pinion.



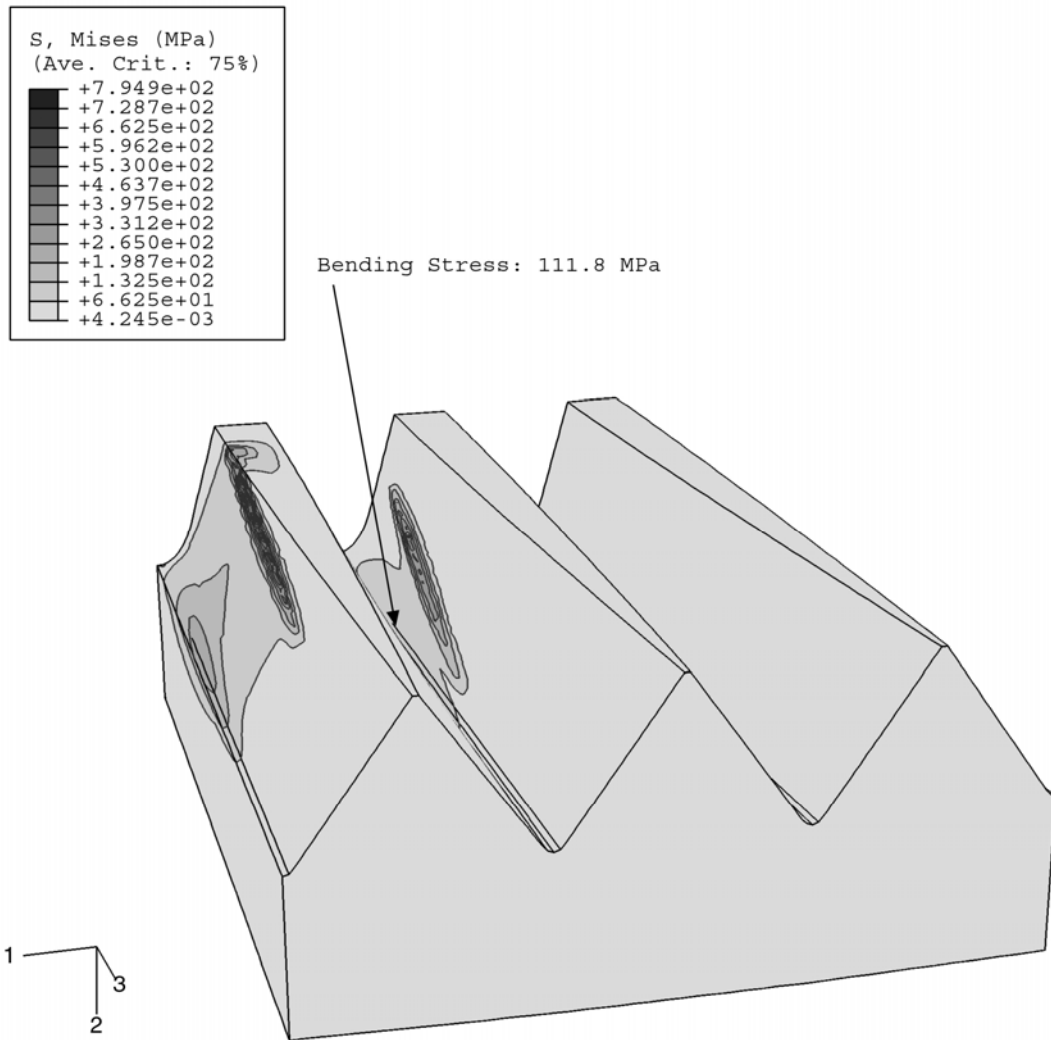
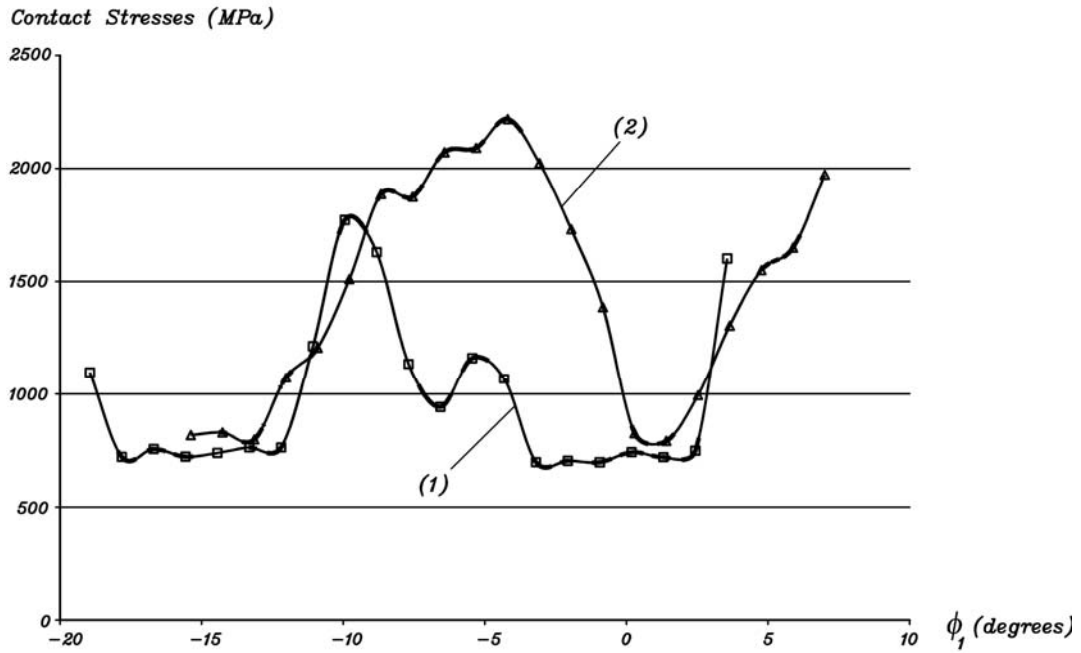
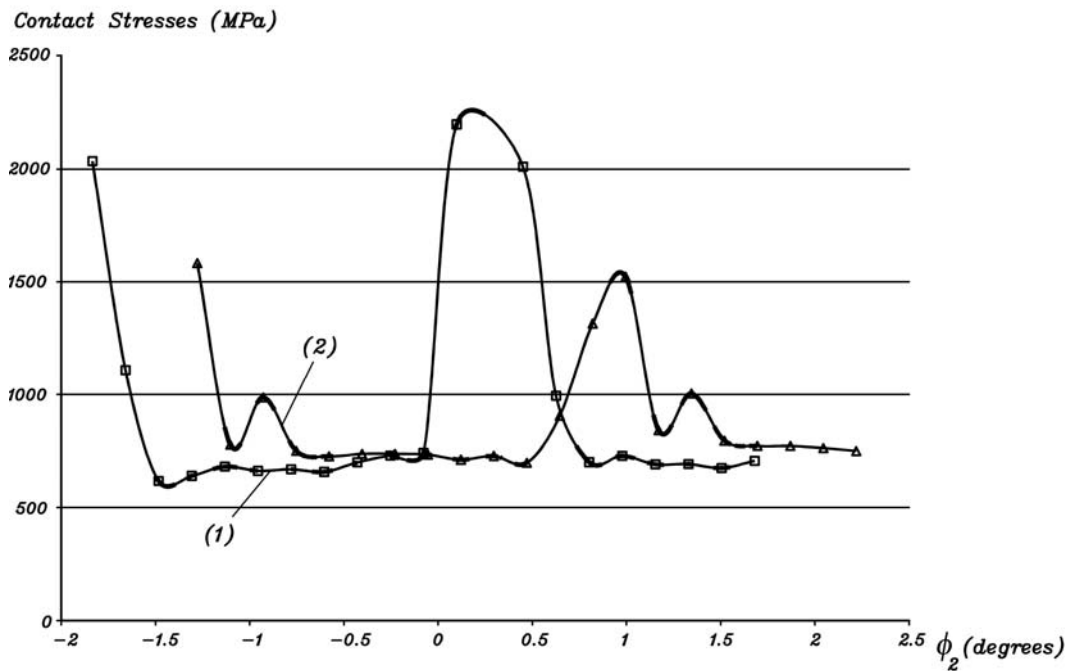


Figure 37.—Contact and bending stresses at a contact point of the face gear of a face-gear drive with spur involute pinion.



(a)



(b)

Figure 38.—Variation of functions of contact stresses during the cycle of meshing in the cases of two face-gear drives: (a) for the pinion and (b) for the gear.

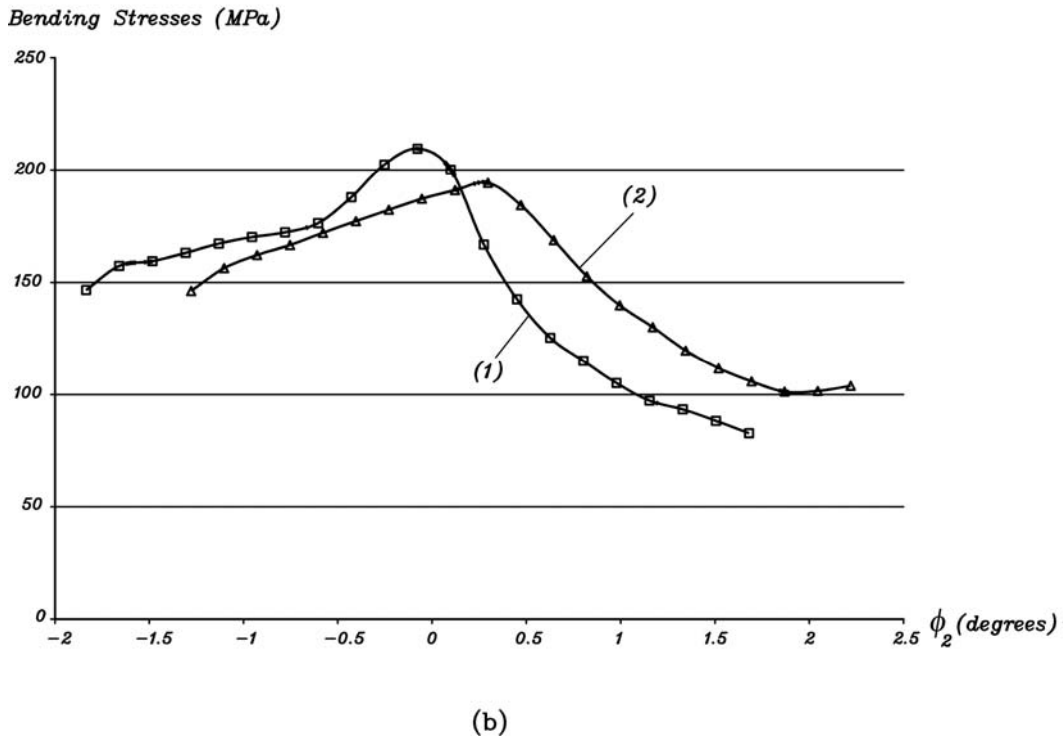
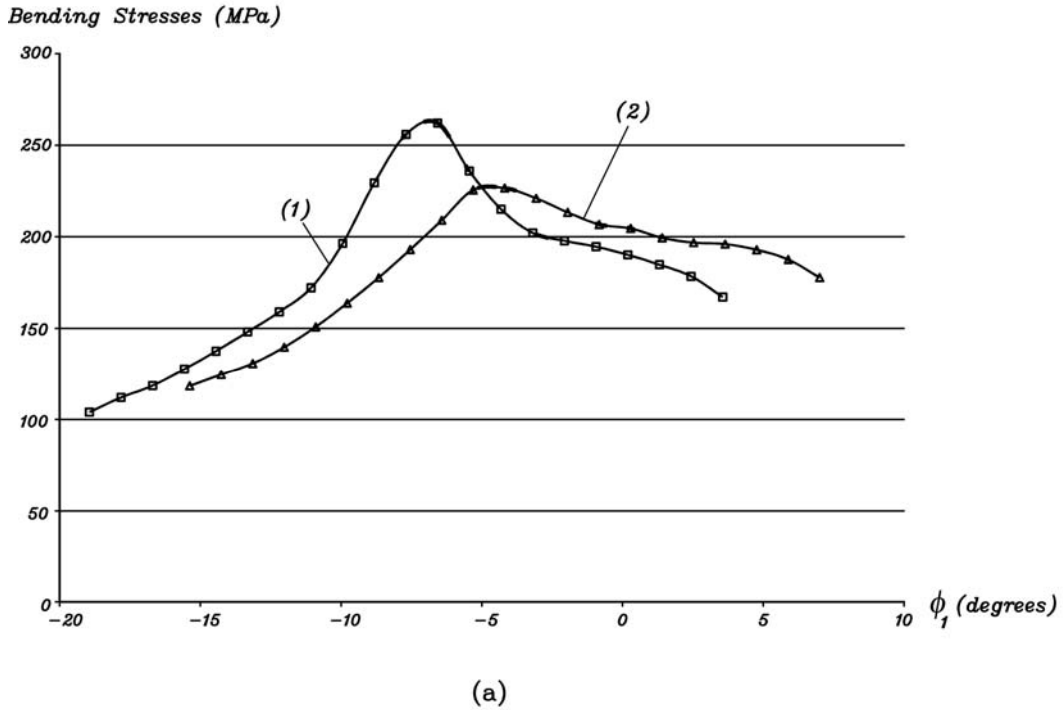


Figure 39.—Variation of functions of bending stresses during the cycle of meshing in the cases of two face-gear drives: (a) for the pinion and (b) for the gear.

# REPORT DOCUMENTATION PAGE

*Form Approved*  
*OMB No. 0704-0188*

Public reporting burden for this collection of information is estimated to average 1 hour per response, including the time for reviewing instructions, searching existing data sources, gathering and maintaining the data needed, and completing and reviewing the collection of information. Send comments regarding this burden estimate or any other aspect of this collection of information, including suggestions for reducing this burden, to Washington Headquarters Services, Directorate for Information Operations and Reports, 1215 Jefferson Davis Highway, Suite 1204, Arlington, VA 22202-4302, and to the Office of Management and Budget, Paperwork Reduction Project (0704-0188), Washington, DC 20503.

<b>1. AGENCY USE ONLY</b> <i>(Leave blank)</i>	<b>2. REPORT DATE</b> February 2005	<b>3. REPORT TYPE AND DATES COVERED</b> Final Contractor Report	
<b>4. TITLE AND SUBTITLE</b>  Face Gear Drive With Helical Involute Pinion: Geometry, Generation by a Shaper and a Worm, Avoidance of Singularities and Stress Analysis		<b>5. FUNDING NUMBERS</b>  WBS-22-714-09-15 NAG3-2450 1L162211A47A	
<b>6. AUTHOR(S)</b>  Faydor L. Litvin, Alfonso Fuentes, Ignacio Gonzalez-Perez, Alessandro Piscopo, and Paolo Ruzziconi		<b>8. PERFORMING ORGANIZATION REPORT NUMBER</b>  E-14979	
<b>7. PERFORMING ORGANIZATION NAME(S) AND ADDRESS(ES)</b> University of Illinois at Chicago Department of Mechanical Engineering 2039 Engineering Research Facility (ERF) 842 West Taylor Street Chicago, Illinois 60607		<b>10. SPONSORING/MONITORING AGENCY REPORT NUMBER</b>  NASA CR-2005-213443 ARL-CR-557	
<b>9. SPONSORING/MONITORING AGENCY NAME(S) AND ADDRESS(ES)</b> National Aeronautics and Space Administration Washington, DC 20546-0001 and U.S. Army Research Laboratory Adelphi, Maryland 20783-1145		<b>11. SUPPLEMENTARY NOTES</b>  Faydor L. Litvin, Ignacio Gonzalez-Perez, Alessandro Piscopo, and Paolo Ruzziconi, University of Chicago, Department of Mechanical Engineering, Chicago, Illinois 60607; and Alfonso Fuentes, Polytechnic University of Cartagena, Department of Mechanical Engineering, Spain. Project Manager, Robert Handschuh, Army Research Laboratory, Vehicle Technology Directorate, NASA Glenn Research Center, organization code RSM, 216-433-3969.	
<b>12a. DISTRIBUTION/AVAILABILITY STATEMENT</b>  Unclassified - Unlimited Subject Category: 37  Available electronically at <a href="http://gltrs.grc.nasa.gov">http://gltrs.grc.nasa.gov</a> This publication is available from the NASA Center for AeroSpace Information, 301-621-0390.		<b>12b. DISTRIBUTION CODE</b>	
<b>13. ABSTRACT</b> <i>(Maximum 200 words)</i>  A new type of face-gear drive with intersected axes of rotation formed by a helical involute pinion and conjugated face-gear has been investigated. Generation of face-gears by a shaper free of undercutting and pointing has been investigated. A new method of grinding or cutting of face-gears by a worm of special shape has been developed. A computerized design procedure has been developed to avoid undercutting and pointing by a shaper or by a generating worm. Also, a method to determine the limitations of the helix angle magnitude has been developed. The method provides a localization of the bearing contact to reduce the shift of bearing contact caused by misalignment. The analytical method provides a simulation of the meshing and contact of misaligned gear drives. An automatic mesh generation method has been developed and used to conduct a 3-D contact stress analysis of several teeth. The theory developed is illustrated with several examples.			
<b>14. SUBJECT TERMS</b>  Gears; Transmissions		<b>15. NUMBER OF PAGES</b> 61	
		<b>16. PRICE CODE</b>	
<b>17. SECURITY CLASSIFICATION OF REPORT</b> Unclassified	<b>18. SECURITY CLASSIFICATION OF THIS PAGE</b> Unclassified	<b>19. SECURITY CLASSIFICATION OF ABSTRACT</b> Unclassified	<b>20. LIMITATION OF ABSTRACT</b>



